

# HIGH-RESOLUTION H-BAND SPECTROSCOPY OF Be STARS WITH SDSS-III/APOGEE. I. NEW Be STARS, LINE IDENTIFICATIONS, AND LINE PROFILES

S. DREW CHOJNOWSKI<sup>1,2</sup>, DAVID G. WHELAN<sup>3</sup>, JOHN P. WISNIEWSKI<sup>4</sup>, STEVEN R. MAJEWSKI<sup>1</sup>,  
MATTHEW HALL<sup>1</sup>, MATTHEW SHETRONE<sup>5</sup>, RACHAEL BEATON<sup>1</sup>, ADAM BURTON<sup>1</sup>, GUILLERMO DAMKE<sup>1</sup>,  
STEVE EIKENBERRY<sup>6</sup>, STEN HASSELQUIST<sup>2</sup>, JON A. HOLTZMAN<sup>2</sup>, SZABOLCS MÉSZÁROS<sup>7,8</sup>, DAVID NIDEVER<sup>9</sup>,  
DONALD P. SCHNEIDER<sup>10,11</sup>, JOHN WILSON<sup>1</sup>, GAIL ZASOWSKI<sup>12</sup>, DMITRY BIZYAEV<sup>2</sup>, HOWARD BREWINGTON<sup>2</sup>,  
J. BRINKMANN<sup>2</sup>, GARRETT EBELKE<sup>2</sup>, PETER M. FRINCHABOY<sup>13</sup>, KAREN KINEMUCHI<sup>2</sup>, ELENA MALANUSHENKO<sup>2</sup>,  
VIKTOR MALANUSHENKO<sup>2</sup>, MOSES MARCHANTE<sup>2</sup>, DANIEL ORAVETZ<sup>2</sup>, KAIKE PAN<sup>2</sup>, AND AUDREY SIMMONS<sup>2</sup>

<sup>1</sup>Department of Astronomy, University of Virginia, P.O. Box 400325, Charlottesville, VA 22904-4325, USA; [drewski@virginia.edu](mailto:drewski@virginia.edu)

<sup>2</sup>Apache Point Observatory and New Mexico State University, P.O. Box 59, Sunspot, NM, 88349-0059, USA

<sup>3</sup>Department of Physics, Austin College, 900 N. Grand Ave., Sherman, TX 75090, USA

<sup>4</sup>Department of Physics & Astronomy, The University of Oklahoma, 440 W. Brooks St., Norman, OK 73019, USA

<sup>5</sup>Department of Astronomy, The University of Texas at Austin, 2515 Speedway, Stop C1400 Austin, Texas 78712-1205, USA

<sup>6</sup>Department of Astronomy, University of Florida, 211 Bryant Space Science Center, Gainesville, FL 32611-2055, USA

<sup>7</sup>ELTE Gothard Astrophysical Observatory, <sup>1</sup>H-9704 Szombathely, Szent Imre herceg st. 112, Hungary

<sup>8</sup>Department of Astronomy, Indiana University, Bloomington, IN 47405, USA

<sup>9</sup>Department of Astronomy, University of Michigan, 830 Dennison, 500 Church St., Ann Arbor, MI 48109-1042, USA

<sup>10</sup>Department of Astronomy and Astrophysics, The Pennsylvania State University, University Park, PA 16802, USA

<sup>11</sup>Institute for Gravitation and the Cosmos, The Pennsylvania State University, University Park, PA 16802, USA

<sup>12</sup>Department of Physics & Astronomy, Johns Hopkins University, Bloomberg Center for Physics and Astronomy, Room 366,  
3400 N. Charles Street, Baltimore, MD 21218, USA

<sup>13</sup>Department of Physics and Astronomy, Texas Christian University, Box 298840, Fort Worth, TX 76129, USA

Received 2014 April 2; accepted 2014 July 25; published 2014 December 3

## ABSTRACT

The Apache Point Observatory Galactic Evolution Experiment (APOGEE) has amassed the largest ever collection of multi-epoch, high-resolution ( $R \sim 22, 500$ ),  $H$ -band spectra for B-type emission line (Be) stars. These stars were targeted by APOGEE as telluric standard stars and subsequently identified via visual inspection as Be stars based on H I Brackett series emission or shell absorption in addition to otherwise smooth continua and occasionally non-hydrogen emission features. The 128/238 APOGEE Be stars for which emission had never previously been reported serve to increase the total number of known Be stars by  $\sim 6\%$ . Because the  $H$  band is relatively unexplored compared to other wavelength regimes, we focus here on identification of the  $H$ -band lines and analysis of the emission peak velocity separations ( $\Delta v_p$ ) and emission peak intensity ratios ( $V/R$ ) of the usually double-peaked H I and non-hydrogen emission lines. H I Br11 emission is found to preferentially form in the circumstellar disks at an average distance of  $\sim 2.2$  stellar radii. Increasing  $\Delta v_p$  toward the weaker Br12–Br20 lines suggests these lines are formed interior to Br11. By contrast, the observed IR Fe II emission lines present evidence of having significantly larger formation radii; distinctive phase lags between IR Fe II and H I Brackett emission lines further supports that these species arise from different radii in Be disks. Several emission lines have been identified for the first time including C I 16895, a prominent feature in the spectra for almost a fifth of the sample and, as inferred from relatively large  $\Delta v_p$  compared to the Br11–Br20, a tracer of the inner regions of Be disks. Emission lines at 15760 Å and 16781 Å remain unidentified, but usually appear along with and always have similar line profile morphology to Fe II 16878. Unlike the typical metallic lines observed for Be stars in the optical, the  $H$ -band metallic lines, such as Fe II 16878, never exhibit any evidence of shell absorption, even when the H I lines are clearly shell-dominated. The first known example of a quasi-triple-peaked Br11 line profile is reported for HD 253659, one of several stars exhibiting intra- and/or extra-species  $V/R$  and radial velocity variation within individual spectra. Br11 profiles are presented for all discussed stars, as are full APOGEE spectra for a portion of the sample.

*Key words:* circumstellar matter – infrared: stars – line: identification – line: profiles – stars: early-type – stars: emission-line, Be

*Supporting material:* machine-readable and VO tables

## 1. INTRODUCTION

Since the first observational description (Struve 1931) of the characteristic double-peaked emission lines of classical Be stars, a wealth of research has demonstrated that the emission lines are formed in geometrically thin, equatorial circumstellar disks fed by gas ejected from the surfaces of rapidly rotating B stars (Porter & Rivinius 2003; Rivinius et al. 2013b). Rapid rotation is certainly involved in the formation of these disks, but a comprehensive model of Be disk formation has yet to be created

and efforts toward one are complicated by factors including the lack of examples of critically rotating Be stars, star-specific peculiarities, and the requirement of an “on/off” switch to the Be phenomenon. For an uncertain but non-negligible fraction of Be stars, the disks are transient, appearing in one epoch but not another (McSwain et al. 2009; Wisniewski et al. 2010). A variable rotation speed ( $v \sin i$ ) that occasionally reaches or exceeds the critical breakup limit is an attractive concept for such a phenomenon (Rivinius et al. 2013c) that needs to be explored

for a sample of transient Be stars. Non-radial pulsation and turbulence due to small-scale magnetic fields remain the most likely mechanisms, along with rapid rotation, responsible for the creation of the disks (Rivinius et al. 2013b). When the disks are present, they appear to undergo Keplerian rotation (Meilland et al. 2007; Wheelwright et al. 2012) and many of the observational signatures are consistent with those predicted by the viscous decretion disk model (Lee et al. 1991; Carciofi et al. 2009; Carciofi 2011).

Multi-wavelength studies of Be disks are particularly valuable for diagnosing their structure because emission at different wavelengths originates from different physical locations within the disks (Carciofi 2011). However, unlike in the optical wavelength regime where they have been extensively studied at high spectral and temporal resolution, only a limited number of Be star surveys have been performed at near-infrared (NIR) wavelengths, and these have typically utilized low spectral resolution (Steele & Clark 2001) and small sample sizes (Murdoch et al. 1994; Clark & Steele 2000; Mennickent et al. 2009; Granada et al. 2010). Detailed NIR spectroscopic studies of individual Be stars are more common (e.g., Hony et al. 2000; Mathew et al. 2012) and have been used to better diagnose the gas distribution within Be disks, including the structure of one-armed density waves (Wisniewski et al. 2007; Štefl et al. 2009; Carciofi et al. 2009).

The Apache Point Observatory Galactic Evolution Experiment (APOGEE; Majewski 2012) is actively providing the first ever bulk view of the high-resolution  $H$ -band properties and variability of Be stars. APOGEE is one of four surveys comprising the Sloan Digital Sky Survey III (SDSS-III; Eisenstein et al. 2011). While the primary goal of the APOGEE survey is to measure the dynamical and chemical history of the Milky Way Galaxy using high-resolution  $H$ -band spectroscopic observations of  $10^5$  red giant branch (RGB) stars, APOGEE devotes 35 fibers per 300-fiber pointing to observe hot stars as telluric standards. This, in addition to the surveys large sky coverage and multi-epoch observing strategy, has made APOGEE ideal for serendipitous Be discoveries and high-resolution NIR time series data of Be stars.

Here, we present the first catalog of APOGEE Be (ABE) stars. An overview of the APOGEE survey and APOGEE data is provided in Section 2, the Be sample is described in Section 3, and the identifications of observed metallic emission lines are discussed in Section 4. Sections 5 and 6 focus on quantitative and comparative analysis of emission double-peak separation ( $\Delta v_p$ ) and double-peak intensity ratios ( $V/R$ ). Commentary on the more unusual or exceptional Be stars within the ABE sample is interspersed throughout, and an atlas of Br11 profiles is provided in Section 7. The Appendix includes supplemental figures displaying full APOGEE spectra for stars with strong emission features, as well as an expanded stellar data table. Future work will focus on the observed spectral variability of sources with multi-epoch APOGEE data as well as follow-up optical spectroscopy for a subset of the sample.

## 2. APOGEE OVERVIEW

### 2.1. APOGEE Instrument and Observations

The APOGEE instrument is a 300 fiber,  $R \sim 22$ , 500 spectrograph (Wilson et al. 2010) attached to the SDSS 2.5 m telescope (Gunn et al. 2006) at Apache Point Observatory.

APOGEE records a vacuum wavelength range of 15145–16955 Å via an arrangement of three Teledyne H2RG 2048 × 2048 detectors. The detector layout consists of “blue,” “green,” and “red” detectors which cover 15145–15808 Å, 15858–16433 Å, and 16474–16955 Å respectively, resulting in coverage gaps between 15808–15858 Å and 16433–16474 Å. Dispersion varies with wavelength, but the central dispersions of the blue, green, and red detectors are  $0.326 \text{ Å pix}^{-1}$ ,  $0.283 \text{ Å pix}^{-1}$ , and  $0.236 \text{ Å pix}^{-1}$  respectively. As with the original SDSS spectrograph (Smee et al. 2013), APOGEE fibers are plugged into custom, pre-drilled aluminum plates which are loaded into the telescope’s focal plane and which can cover  $3^\circ$  diameter areas of sky. Each fiber has a  $2''$  field of view.

The APOGEE survey uses the Two Micron All Sky Survey (2MASS; Skrutskie et al. 2006) as a source catalog and focuses on observations of known or photometrically likely RGB stars for its main science objective (230/300 fibers per plate). For calibration purposes, blank sky (35/300 fibers) and blue telluric standards (35/300 fibers) are also observed. Typical exposure times are 1 hour, and the number of repeat observations per field is approximately equal to the number of 1 hour observations needed to reach a combined signal-to-noise ratio (S/N) per raw pixel of 100 for stars at the field-specific  $H$  magnitude limit. The bright limit for science targets is always  $H = 7.0$ , while the faint limit is variable and can be  $H = 11.0$  (1 hour visit),  $H = 12.2$  (3 1 hour visits),  $H = 12.8$  (6 1 hour visits),  $H = 13.3$  (12 1 hour visits), or  $H = 13.8$  (24 1 hour visits). Cohorts of RGB targets with similar  $H$  magnitudes are exchanged in and out of the observing sequence as  $S/N \sim 100$  is reached.

### 2.2. APOGEE Telluric Standard Stars

Hot O- and B-type (OB) stars are ideal candidates for telluric standard stars (TSS’s) in the  $H$  band because the associated spectra are relatively featureless (Meyer et al. 1998; Steele & Clark 2001). Selection of the TSS for each APOGEE field is based on  $H$  magnitude and non-reddening-corrected color rather than on intrinsic spectral properties (Zasowski et al. 2013), such that the TSS for a given field are simply the apparent bluest available stars. Thus, APOGEE makes no distinction between “normal” and emission-line stars other than to prevent from selection as TSS any stars that are reddened with respect to other stars (e.g., dusty B[e] stars) in the  $3^\circ$  fields.

Unlike the RGB science targets, TSS are restricted to  $5.5 \leq H \leq 11.0$  and are therefore always expected to reach  $S/N \geq 100$  in the typical hour exposures. In addition, the TSS for each APOGEE field are generally “locked-in,” meaning that they are observed every time their respective fields are observed rather than being traded in and out of the sequence as are the RGB stars. A more comprehensive description of TSS selection is presented in Zasowski et al. (2013).

### 2.3. Apache Point Observatory Galactic Evolution Experiment Spectra

There are several details worth noting about the APOGEE spectra. Vacuum wavelengths given in angstroms (Å) are used in APOGEE data and throughout this paper. Some of the spectra were recorded during APOGEE commissioning, prior to the instrument having achieved optimal focus. The resolution of red detector data in APOGEE spectra taken prior to MJD < 55804 (September 2011) is  $R \sim 16,000$ ,

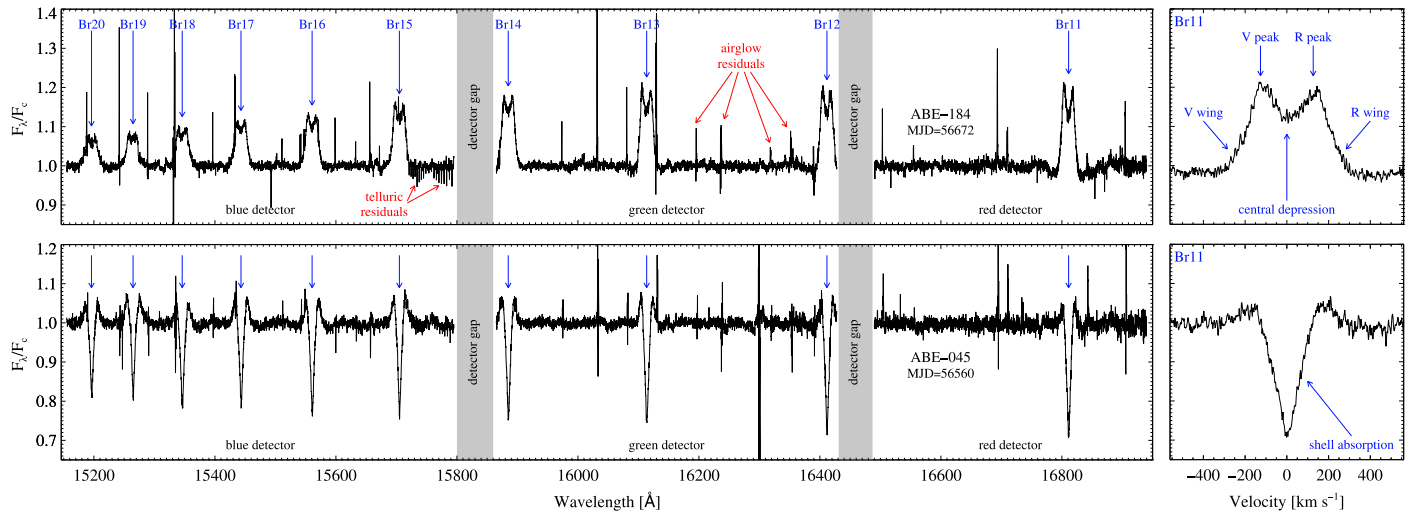


**Figure 1.** Two examples of APOGEE spectra of Be stars. The “red,” “green,” and “blue” detectors and the gaps between detectors are labeled in the left panels and examples of residuals from the airglow and telluric removal process airglow residuals are labeled in the upper left panel (red arrows and text). The APOGEE Be star designations (ABE-184 and ABE-045) are shown along with the modified Julian date (MJD) of observation, and the Brackett series lines are labeled (blue arrows and text). Right-hand panels show the Br11 profiles on a velocity scale: ABE-184 exhibits a typical Be star line profile, where the central depression is a consequence of the disk geometry (e.g., Huang 1972), while the Brackett lines for ABE-045 are dominated by shell absorption resulting from occultation of the star by the disk in a nearly or exactly edge-on system (e.g., Rivinius et al. 2006).

while the resolution is  $R \sim 22,500$  for all blue and green detector data regardless of date and for all post-55804 red detector data. The raw data is processed by an automated reduction pipeline (Nidever, in preparation) that extracts the spectra, performs flat-field and wavelength calibration, and performs sky and telluric corrections. APOGEE’s reduction pipeline is designed to use sky and TSS exposures (see Section 2.2) to remove airglow and telluric absorption lines from the high-resolution spectra. Because the airglow removal process has not yet been perfected, residuals from partially subtracted airglow lines remain in the final reduced data products.

Since the APOGEE survey focuses on chemical abundance and radial velocity (RV) analysis, flux standard stars are not observed and therefore the spectra are not flux-calibrated. All spectra displayed in this paper were continuum normalized using the CONTINUUM task in IRAF by fitting low-order splines to sections of blank continuum adjacent to H $\alpha$  Brackett lines, separately for each detector. Quoted emission line intensities and V/R intensity ratios refer to intensity relative to normalized continuum level ( $F_{\lambda}/F_c$ ). Due to the proximity of the Br12 and Br14 lines to the coverage limits of the green detector (21 and 27 Å respectively), it was at times difficult to achieve a continuum fit that did not result in obviously incorrect intensity levels for those with respect to the other Brackett lines. The tendency of the full-width at continuum level for Brackett series emission lines to well exceed  $1000 \text{ km s}^{-1}$  was a further complication in salvaging the Br12 and Br14 lines, which are de-emphasized from analysis for these reasons.

Figure 1 displays examples of APOGEE spectra for two newly-discovered Be stars, demonstrating the three-detector arrangement and associated coverage gaps. The ABE star IDs and modified Julian dates (MJD) of observation are provided above or below “red detector” continuum level, and commonly observed emission lines (see Section 3.5) are labeled with blue text and arrows. Examples of airglow residuals are noted with red text and arrows. The right-hand panels show Br11 line profiles from the same spectra on a velocity scale, with the line profile features of interest

labeled. In most cases, Br11 is the strongest hydrogen line covered as well as the hydrogen line least likely to be affected by airglow or telluric contaminants should those be a significant issue. In subsequent figures, narrow contaminants (airglow and hot/cold/bad pixels) have been carefully trimmed from the spectra so as to avoid distraction from the features of astrophysical importance.

#### 2.4. Public Availability of the Spectra

Both proprietary and publicly available spectra are used and displayed in this paper. The publicly available spectra were included in SDSS data release 10 (DR10: pertains to APOGEE data taken prior to MJD = 56112), and the full data set will be made publicly available in SDSS data release 12 (DR12: scheduled for 2014 December). Shortly after DR12, we intend to convert the ABE star spectra to the format accepted by the Be Star Spectra Database (BeSS; Neiner et al. 2011) and deposit them there, ensuring convenient public access. More details on DR10-released APOGEE data can be found on the SDSS-III website (<https://www.sdss3.org/dr10/irspec/>).

### 3. THE ABE SAMPLE

#### 3.1. Sample Description

The sample at hand consists of 238 Be stars that have been observed by APOGEE a total of 1082 times. Of the 238 ABE stars, 202 were identified through periodic visual inspection of APOGEE spectra and 36 were targeted intentionally to expand the subset of previously known Be stars.

We measured the velocity separations ( $\Delta v_p$ ) of the violet (V) and red (R) emission peaks of all lines with well-defined peaks in all spectra of sufficient quality (typically  $S/N > 50$ ; dependent on emission strength) using the SPLOT feature of IRAF. Measurements pertaining to emission peaks coincident in wavelength position with strong airglow lines or diffuse interstellar bands (DIBs) (see Section 4.1) were thrown out.

**Table 1**  
List of ABE Stars

ABE ID	2MASS Designation	Star Name	2MASS $H$ (mag.)	Lit. Spectral Type	Ref.	$\Delta v_p$ Br11 (km s <sup>-1</sup> )
001	20212485+3722482	VES 203	9.108	B0.5Ve	74	208
002	20151525+3654562	HD 228576	9.888	Ae	29	152
003	20162816+3703229	HR 7757	6.548	B6IIIe	22	305
004	20234596+3830033	HD 229221	6.734	B0.2IIIe	66	115
005	20184170+3759106	Hen 3-1876	9.699	OB	6	271
006	19124025-0627316	HD 179405	8.084	B2Ve	68	294
007	19104149-0542581	HD 178920	9.236	B8II/III	58	181
008	18000176-2323071		10.699			233
009	20461437+5039005	TYC 3586-282-1	9.192	(B8)	C	175
010	20450869+5033004	BD+50 3188	9.311	(B)	C	138
011	20535693+5005293	TYC 3583-670-1	9.698			252
012	20554731+5040274		10.766			115
013	18574179-0419113	EM* CDS 1038	10.428	OB	24	bl
014	21300088+4529390	HD 204860	6.931	B5.5Ve	60	326
015	18123846-2708292	HD 166629	9.155	B5nne	41	70
016	18185069-1227145	HD 168135	7.406	B8Ve	59	238
017	18122758-1546123	BD-15 4863	9.695	Be	24	376
018	18194798-1724130		10.976			sp
019	23533653+5649116	HD 223924	8.177	B1.5:III:n	25	296
020	18432516-0339100	SS 412	10.528	OB:e	33	217
021	04220085+5430434	HD 232940	8.625	(B9)	C	291
022	04254177+5615294	TYC 3727-1849-1	9.438			495
023	03282223+4507560	BD+44 709s	10.546	OB	14	386
024	05113282+2408029	TYC 1846-17-1	9.596	(A3)	C	158
025	05452088+2909281	HD 247042	9.165	O9.5:	15	346
026	05485364+2908100	HD 38708	8.015	B3:e:psh	8	324
027	05453713+3007253	TYC 2405-1358-1	9.825			489
028	06123985+3258216	HD 42529	8.090	B9V	57	297
029	06165595+3414299	HD 254168	9.169			301
030	06185921+3413502	HD 43681	8.806	(A2)	39	333
031	06273614+1815476	HD 257473	9.378	B5e	5	133
032	22252246+5642384	SS 453	10.200	Be:	33	508
033	23181131+5550356	HD 240249	9.250	(B8)	C	205
034	23521212+6710073	MWC 1085	8.787	(B3Ve)	54	551
035	06334350-3202486	Hen 3-14	9.650	B	24	241
036	06283925-3222165	HR 2364	6.113	B3Ve	69	456
037	05590290+3101488	HD 40254	9.210	(B8)	39	234
038	20032620+2242411	HD 345589	10.595	(A3)	52	224
039	18000839-2356576	SS 338	9.647	B8e:	33	259
040	17375482-2457569	HD 159845	6.773	B3IIIe	45	99
041	18382765-1014211		10.640			141
042	18464650-1021523	BD-10 4799	10.094	(B)	C	181
043	17441414-2727284	HD 161004	7.880	B9IVe	41	290
044	17432344-2715411	HD 316179	7.673	Be:	35	247
045	01542524+5651061	TYC 3692-1234-1	10.321			344
046	02135183+5354525	HD 13544	9.055	B0.5III:n	27	294
047	05390426+3758359	HD 37266	7.309	B8V	57	250
048	21375002+4258309	BD+42 4162	8.916	(A0)	39	333
049	21103095+4741321	HR 8107	6.360	B6IV	22	197
050	19584848+2305215	HD 345439	10.629	B2Vpe	77	1153
051	19571220+2158541	HD 345439	9.869	(A0)	52	373
052	18052711-2921573	TYC 6854-2016-1	10.009	(B8)	61	405
053	18023404-3027418	HD 317026	9.467	(B9)	52	216
054	05064093+2230389	HD 32811	6.523	B8.5V	57	315
055	06591343+0427179	HD 51893	9.077	B9V	58	344
056	00302445+6010093	HIP 2382	9.710	B6III	48	as(sh)
057	02534457+6443068	TYC 4056-415-1	9.293	(B5)	61	sh
058	18072725-2506165	HD 165517	6.967	B0Iae	45	tc
059	18144388-2137597	HD 167113	9.030	(B9IV:)	61	415
060	07134058+3806302	HD 55200	8.297	(A0)	39	sh
061	04361726+5230217	HD 28942	8.159	Ash	44	sh

**Table 1**  
(Continued)

ABE ID	2MASS Designation	Star Name	2MASS $H$ (mag.)	Lit. Spectral Type	Ref.	$\Delta v_p$ Br11 (km s <sup>-1</sup> )
062	03030934+6654223	TYC 4060-96-1	8.398			456
063	06351041+0634180	HD 260153	9.417	B8III	42	w
064	18451050-0545120	TYC 5126-2325-1	10.733			291
065	18434859-0608188	HD 173075	9.358	B9IV	58	235
066	18402120-0455127	TYC 5121-940-1	10.299			187
067	03292627+4656162	HR 1047	5.902	B7Vne	51	133
068	17224642-2533273	HD 157174	8.488	A0IV	45	208
069	18274975-1104312		10.165			238
070	18251991-0918163	BD-09 4724	9.550	(A0IV)	C	w
071	18424368-1000273	TYC 5696-503-1	10.454	Be	33	138
072	18043735+0155085	HD 165174	6.224	B0IIIIn	22	w
073	22583631+5528116	BD+54 2887	9.538	(A0)	61	193
074	19233702+3859363	HD 182550	8.818	B8V	47	66
075	03464087+3217247	HD 23478	6.486	B3IVe	10	913
076	04432066+4754385	VES 828	10.896			301
077	04423114+3830469		10.455			162
078	21351726+5647589	TYC 3975-1585-1	10.101	B8	12	400
079	07081479-2325541	HD 54551	8.775	B1.5II	45	524
080	20282074+4526025	BD+44 3475	9.451			sh
081	00104514+5801058	HD 628	7.521	(B9)	39	205
082	05540108+1241033	BD+12 938	10.172			250
083	05453721+1311210	HD 247299	9.987	(A0)	62	119
084	01042742+5756263	HD 236611	8.978	(A)	C	265
085	01183306+5822304	HD 236689	8.853	B1.5V:epsh	8	321
086	01355734+5809128	TYC 3683-1262-1	9.840			209
087	07331124-1136421	HD 60260	9.232	B3Ve	58	129
088	01055296+6558158	HD 6343	6.843	B5Vn:e	20	115
089	00573323+6709339	TYC 4029-428-1	9.595			342
090	00501808+6710377	BD+66 64	8.588	(B9)	C	sh
091	05564423+1601018	HD 39984	9.140	(A2)	39	115
092	03250006+5029394	TYC 3320-1906-1	9.425	B7	9	417
093	00080292+7332356	TYC 4306-1125-1	9.115	B8V	37	337
094	00331160+5140069	HD 232214	8.855	(B8)	C	92
095	06272285+0824429	HD 45396	8.907	(A2)	39	w
096	06300018+0817453	HD 45828	8.506	(B8?)	C	w
097	05164674+3022455	HD 34193	8.498	(AOe)	39	203
098	23152849+6416002	HD 219523	7.218	B5V	36	301
099	06073989+2751354	HD 41639	8.599	B6Vne:	38	578
100	05341240+4516410	HD 36467	8.167	B9III	37	300
101	05124298+4754272	BD+47 1108	9.581	(A0)	39	326
102	05003547+3552170	TYC 2400-1784-1	10.396			273
103	17494627-2249517		10.473			<61
104	18411366-0247380	BD-02 4698	8.853	(B)	C	sh?
105	20451060+5112379	HD 235350	8.652	B0.5IV	8	502
106	02250591+5515032	TYC 3690-1236-1	10.581			480
107	21563126+5041249	TYC 3617-2074-1	10.112			233
108	06185755+2323286	HD 254842	8.631			185
109	06231994+2506057	HD 256137	9.734	(A2)	39	106
110	04365908+5217135	HD 29035	7.930	B9.5Ve	64	w
111	18581515-0528567	AS 332	9.639	Be	43	w
112	04321707+4816572	HD 28543	7.725	(A0)	39	w
113	04363913+4104368	HD 29096	7.323	B8IV	57	333
114	04460607+4705516	TYC 3347-1615-1	10.713			sh?
115	20185676+3745319		11.326			139
116	17331509-1922379	HD 159032	8.725	B9IV	45	387
117	17515926-3029411	HD 162345	8.291	(B8)	39	128
118	17534729-2945087	HD 316573	9.850	(B9)	52	115
119	17531191-2857284	AS 251	9.961	B	24	259
120	17521395-2744257	HD 316475	9.225	(B9)	39	282
121	17525570-2218434	TYC 6262-3203-1	9.292			166
122	18194176-1058093	TYC 5681-507-1	10.027	(A5)	62	179

**Table 1**  
(Continued)

ABE ID	2MASS Designation	Star Name	2MASS $H$ (mag.)	Lit. Spectral Type	Ref.	$\Delta v_p$ Br11 (km s <sup>-1</sup> )
123	18220126-1048042	TYC 5681-151-1	10.614			177
124	18161427-2906365	HD 167401	9.322	B4II/III	41	627
125	18221389-1307360	TYC 5689-54-1	10.273			<60
126	18245968-1406408	HD 169418	8.995	B9.5III	45	326
127	18205460-1243598	HD 168566	8.710	B9III	45	114
128	18404465-0758241	HIP 91591	8.825	B8Ve	49	276
129	18385819-0827466	GSC 05692-00540	10.451	B7	17	267
130	18405017-0741018	GSC 05692-00399	10.508	B7	17	423
131	18395898-0733138	BD-07 4647	9.642	B5	17	143
132	18355878-0744307	BD-07 4630	8.963	B9	17	w
133	17500331+4823391	88 Her	6.913	B6IIIInpsh	53	285
134	18295996-0908375		10.761			198
135	18432970-0919127	HD 173010	7.179	O9.7Ia	73	sh?
136	18064578-2821496	HD 165365	7.024	B7.5III	41	232
137	18042703-2228572	NGC 6531 F195	11.130			<25
138	19150144+0948272	HD 180126	7.565	B2IV	68	365
139	19164642+1058468	HD 180587	7.578	ApsH	18	sh
140	20234436+3728351	HR 7807	6.228	B2Vne	63	382
141	21061887+2824477	HD 201036	8.996	B6/8Vn	38	247
142	19270008+1632172	HD 183035	7.844	A0V	70	320
143	20040584+3009117	HD 333378	10.150	(A0)	52	313
144	20005874+3113497	HD 189847	7.122	B7V	16	260
145	17530194-2219531	TYC 6262-1413-1	9.926			sh?
146	06072002+2640558	HD 41600	7.132	B9IV	57	w
147	19424993+4239003	HD 186485	8.484	B9V	34	123
148	20002133+2135515	HD 345506	9.683	(B8)	52	sh?
149	03434449+3143092	IRASF03406+3133	10.780			sp
150	18412551-0534033		10.902			388
151	18404500-0740458	TYC 5692-1370-1	10.799	B7	17	137
152	07290132-0832539	SS 120	10.733	B8e:	35	461
153	17221970-2833450		10.940			sh
154	05394249+2215279	TYC 1310-2084-1	9.969	(B8)	61	360
155	01590196+5725521	TYC 3692-1671-1	10.611			819
156	23380341+5556420	HD 222185	8.343	(A2)	39	w
157	19450599+1617091	HD 186637	7.937	(B9e)	39	359
158	21520306+5853123	AS 478	9.792			87
159	22275192+6300090	MWC 1062	8.804	B5:e	3	265
160	21365704+6811073	HD 206135	7.811	B3V	21	316
161	21551055+5326166	TYC 3968-1354-1	10.574	OB-	14	422
162	06063872+2754038	BD+27 981	9.960	(B8)	62	219
163	22465987+5345241	HD 215837	8.104	(A0)	39	357
164	22202269+5151395	HD 212044	7.702	B1:V:nneP	8	191
165	22245295+5207583	HD 212666	8.681	B5.5e	59	397
166	06460565-0558109	TYC 4812-2496-1	9.971			308
167	06495552-0530472	HD 49787	7.836	B1Ve	68	300
168	06570947-0832309	HD 51477	8.223	B3Ve	58	628
169	06024105+2202482	HD 40897	8.000	(B9)	39	255
170	06014161+2224036	HR 2116	6.400	B8V	26	153
171	06081219+2156586	TYC 1326-1188-1	10.257	(A2)	62	362
172	05212545+1601440	HD 34906	8.641	(B9V)	61	142
173	05175643+1519211	TYC 1283-1360-1	10.617			sh
174	05240938+1633455	HD 35269	7.552	A0V	76	448
175	05214456+1709194	TYC 1300-652-1	10.731			w
176	05133229+3806348	HD 33656	9.215	B5	2	551
177	05194374+3820304	HD 280849	9.654	(B3)	52	522
178	06450343-0034140	CoRoT 102762536	11.651	B1V	75	sp
179	06450928-0115205	EM* RJHA 51	10.563	B5Ib	75	243
180	06422978+0053582	EM* RJHA 40	10.613	B3Ib	75	183
181	05355408-0537423	HD 37115	7.204	B7.5V	58	238
182	06123495+4145095	TYC 2934-118-1	10.240			376
183	07364229-1303499	HD 60993	9.131	B2II	45	348

**Table 1**  
(Continued)

ABE ID	2MASS Designation	Star Name	2MASS $H$ (mag.)	Lit. Spectral Type	Ref.	$\Delta v_p$ Br11 (km s <sup>-1</sup> )
<b>184</b>	05361555+3257145	HD 245174	9.790	(B3)	62	268
<b>185</b>	05580029+2437017	HD 40132	7.564	B9	19	85
<b>186</b>	07075533+0143105	HD 54167	9.672	B5/7Ib:	58	328
187	06121659+2005097	HD 253214	8.917	B1.5:V:nn	8	220
188	06121386+2000034	HD 253215	10.444			298
189	07370572+1654153	HD 60848	7.071	O9.5IVe	67	305
<b>190</b>	06110671+1810591	HD 252904	9.089	B9V	11	w
191	18084894-1858344	HD 165854	7.903	B9e	59	274
<b>192</b>	18103823-1910006	HD 166291	8.303	B3II	45	272
193	18011841-2721498	SS 339	10.713	B8e:	33	250
<b>194</b>	18173492-1842282	HD 313062	9.676			327
195	19120326+0237212	HD 179343	6.613	B8III	68	266
196	05010612+4134002	HD 277241	10.836	B8	13	w
197	18095327-2302251	HD 166055	9.662	(B9)	62	221
<b>198</b>	18091443-2246378	HD 165894	8.183	B3IV/V	45	158
<b>199</b>	17554711-2142367	TYC 6262-371-1	9.301			164
<b>200</b>	18235550-1547477	Lan 671	9.976			280
<b>201</b>	18282453-1642195	BD-16 4888p	9.825			138
<b>202</b>	18283909-1512088	TYC 6266-143-1	10.487			w
A01	00201742+6227498	MWC 5	8.025	B0.5IV	7	122
A02	00320285+6709401	HD 2789	7.519	B3:Vne	23	320
A03	04042164+5319447	MWC 80	7.165	B1Vnnpe	8	as
A04	05251782+2936535	HD 35347	7.948	B2:nne	38	268
A05	05445623+2127384	HD 38191	8.380	B1:V:ne:	8	246
A06	05503228+1801349	HD 39018	7.898	(B9)	39	w
A07	06183944+2300285	HD 43703	7.475	B1IV:p?	8	w
A08	06330559+1656553	HD 46264	7.522	B5Vne	31	409
A09	06333223+0820080	HD 259597	7.779	B1Vnne	28	289
A10	06525305-1000270	HD 50424	8.971	B8e	35	178
A11	06545882-0342013	HD 50891	7.880	B0.5Ve	68	215
A12	06561908-0348254	HD 51193	8.039	B1.5IVe	68	358
A13	06574289+1754071	HD 51354	7.183	B3Vn	40	257
A14	07093697-1605467	HD 54786	9.051	B1.5Ib:	45	256
A15	07133410-0204390	HD 55606	8.704	B0.5Vnnep	69	237
A16	19525141+2214226	HD 345122	8.963	B3Ve	46	233
A17	20024644+2151160	HD 190150	8.186	B6IV-Ve	40	241
A18	21082962+4715254	HD 201522	8.022	B0V	16	
A19	21250244+4427063	MWC 640	7.206	B1.5V:nnep	8	205
A20	21291483+4420173	HD 204722	7.643	B1.5IV:np	25	358
A21	22013820+5010046	MWC 649	8.701	B3e	1	109
A22	22060834+4954088	AS 483	9.631	B1.5V:nne:	8	362
A23	18211606-1301256	MWC 922	7.396	unclB[e]	55	sp
A24	05181018+3739003	HD 34302	7.534	(B8)	39	163
A25	05231490+3742536	HD 280999	9.582	(B3)	52	214
A26	05254477+3538499	HD 35345	7.851	B1Vep	7	sp
A27	05280968+3516540	EM* CDS 496	8.669	OB	24	w?
A28	05595354+2505190	HD 250028	8.083	B2:V:nep	32	288
A29	05530609+2626435	HD 39340	7.579	B3Ve	59	197
A30	05533110+2544321	HD 248753	7.361	B2:Vnne	23	279
A31	05535984+2625212	HD 39478	7.691	B2Ve	59	242
A32	06072661+2205477	IGR J06074+2205	10.189	B0.5Ve	71	380
A33	06074953+1839264	EM* LkHA 208	9.834	A7e	65	sp?
A34	06065436+1902040	HD 251726	7.644	B1V:e	8	159
A35	06184553+1516522	MWC 137	7.840	sgB[e]	56	57
A36	06135416+1631049	HD 253659	8.327	B0.5:V:nne	8	312
Q01	20240654+3829332	HD 229239	7.093	B0.2III	66	
Q02	20194162+3811060	HD 228932	9.386	B	35	
Q03	20213867+3725151	BD+36 4032	7.566	O8.5V	66	
Q04	20213589+3721395	Hen 3-1885	10.855	A0V	30	
Q05	06382991+0042351	HD 291946	9.321	B9	2	

**Table 1**  
(Continued)

ABE ID	2MASS Designation	Star Name	2MASS $H$ (mag.)	Lit. Spectral Type	Ref.	$\Delta v_p$ Br11 (km s <sup>-1</sup> )
Q06	18071193-2516305	HD 315177	10.022			
Q07	19582996+2033006	HD 350989	10.534	B7III <sub>n</sub>	50	
Q08	20012170+2217258	HD 345475	9.484	B0	4	
Q09	23204452+6111404	EM* CDS 1459	7.471	O6.5(f)(n)p	72	
Q10	00350607+6258585	EM* CDS 53	10.369	OB-e:	14	
Q11	00310135+5539101	HD 232208	9.519	B3:e	3	
Q12	00255124+7148258	HD 2083	7.041	O9.5III	34	
Q13	01243585+5812454	EM* CDS 144	10.499	OB-e:	14	
Q14	04310304+4146289	HD 276414	10.148	(B8)	52	
Q15	04390489+4115001	HD 29332	8.246	B3ne	1	
Q16	05085056+4144262	HD 32961	8.970	B2	13	
Q17	04360336+3640031	HD 280006	7.747	A0Ib:	33	
Q18	06321639+0110289	HD 288805	9.611	B5	2	
Q19	06594264-1109265	HD 52159	9.793	B3Vne	69	
Q20	05204307+3726192	HD 34656	6.634	O7.5(f)II	73	
Q21	07213463-0553498	HD 57539	6.834	B3IV	58	
Q22	06154017+0603582	HR 2231	6.336	B6Ve	69	
Q23	22061730+6355026	EM* CDS 1299	10.236	OB	24	

**References.** (1) Merrill et al. (1942); (2) Cannon & Mayall (1949); (3) Merrill & Burwell (1949); (4) Popper (1950); (5) Miller & Merrill (1951); (6) Nassau & Harris (1952); (7) Morgan et al. (1953); (8) Morgan et al. (1955); (9) Heckmann et al. (1956); (10) Hiltner (1956); (11) Duflot et al. (1958); (12) Alknis (1958); (13) McCuskey (1959); (14) Hardorp et al. (1959); (15) Bouigue et al. (1961); (16) Fehrenbach et al. (1962); (17) Roslund (1963); (18) Feast & Thackeray (1963); (19) McCuskey (1967); (20) Schmidt-Kaler (1967); (21) Racine (1968); (22) Lesh (1968); (23) Guetter (1968); (24) Wackerling (1970); (25) Walborn (1971); (26) Cowley (1972); (27) Lesh & Aizenman (1973); (28) Turner (1976); (29) Henize (1976); (30) Voroshilov et al. (1976); (31) Davis (1977); (32) Christy (1977); (33) Stephenson & Sanduleak (1977); (34) Hill & Lynas-Gray (1977); (35) Stephenson & Sanduleak (1977); (36) Roman (1978); (37) Bartaya (1979); (38) Clausen & Jensen (1979); (39) Ochsenbein (1980); (40) Jaschek & Jaschek (1993); (41) Houk (1982); (42) Voroshilov et al. (1985); (43) Bopp (1988); (44) Bidelman (1988); (45) Houk & Smith-Moore (1988); (46) Radoslavova (1989); (47) Sato & Kuji (1990); (48) Turner et al. (1992); (49) Grillo et al. (1992); (50) Turner (1993); (51) Garrison & Gray (1994); (52) Nesterov et al. (1995); (53) Abt & Morrell (1995); (54) Kohoutek & Wehmeyer (1997); (55) Lamers et al. (1998); (56) Esteban & Fernandez (1998); (57) Grenier et al. (1999); (58) Houk & Swift (1999); (59) Yudin (2001); (60) Chauville et al. (2001); (61) Kharchenko (2001); (62) Fabricius et al. (2002); (63) Abt et al. (2002); (64) Miroshnichenko et al. (2003); (65) Hernández et al. (2004); (66) Negueruela (2004); (67) Negueruela et al. (2004); (68) Frémat et al. (2006); (69) Levenhagen & Leister (2006); (70) Uzpen et al. (2007); (71) Reig et al. (2010); (72) Walborn et al. (2010); (73) Sota et al. (2011); (74) Mathew & Subramaniam (2011); (75) Sebastian et al. (2012); (76) Chargeishvili et al. (2013); (77) Eikenberry et al. (2014).

No attempt was made to remove underlying photospheric absorption prior to  $\Delta v_p$  measurement.

Table 1 provides the ABE identifiers, star names, 2MASS  $H$  magnitudes, literature spectral types and references where available (see Section 3.2), and the mean  $\Delta v_p$  for the Br11 line from all APOGEE spectra for each source. Star names beginning with “J” are 2MASS designations, and newly identified Be stars are indicated by bold font for the ABE ID. If a  $\Delta v_p$  measurement for the Br11 line could not be made in any of the available spectra despite evidence of Br11 emission or shell absorption, one of the following abbreviations is provided in place of a  $\Delta v_p$  value: “w” weak emission-peaks not discernible; “sp” single-peaked emission; “sh” shell absorption without resolved adjacent emission peaks; “as” severe asymmetry in emission peak heights such that only one peak is discernible (not the same as single-peaked); “bl” V peak of Br11 is severely blended with Fe II 16792 (ABE-013); “tc” spectra are heavily contaminated by telluric features (ABE-058).

The ABE identifiers were assigned to avoid the use of sometimes lengthy survey identifiers which are the only star names available. Three groups of ABE stars are distinguished from one another by ABE ID as follows:

(1) **ABE-001–ABE-202** refer to Be stars that were quasi-randomly targeted by APOGEE as TSS and subsequently identified as Be stars through visual inspection of the wavelength region encompassing Br11 and Fe II 16878. To

account for sources only producing emission lines in certain epochs, which was frequently the case, it was necessary to examine all >70, 000 individual spectra for all >17, 000 telluric stars.

(2) **ABE-A01–ABE-A36** refer to Be stars that we targeted intentionally via internal proposals for APOGEE observations of ancillary (hence the “A” prefix of the ABE IDs) science targets falling within a subset of pre-planned APOGEE fields. Most of the intentionally targeted Be stars are early-type (B3 and hotter) classical Be stars, showing stronger than average  $H$ -band emission in the APOGEE spectra, but two stars classified as B[e] in the literature were observed (ABE-A23 and ABE-A35) as was a reported Herbig Ae star (ABE-A33).

(3) **ABE-Q01–ABE-Q23** refer to stars which (a) had existing “emission line star” classifications in the literature, (b) appeared to be hot OBA stars in the APOGEE spectra, but (c) did not produce any discernible emission in any of the associated APOGEE data (all have multi-epoch data), or in others words, were  $H$ -band quiescent (hence the “Q” of the ABE IDs) during the observations.

### 3.2. Literature Spectral Types

The He I 17007 line, analogous to optical He I in terms of utility as an effective temperature ( $T_{\text{eff}}$ ) diagnostic for OB stars

(Blum et al. 1997; Meyer et al. 1998) and the only non-hydrogen stellar absorption feature expected to be present for B-type stars (the earliest-O stars exhibit He II 15723, 16923 absorption), is not covered by APOGEE spectra. Therefore, detailed spectral classification of OB stars is not possible with these data and the literature was perused for the existing spectral classifications included in Table 1.

The Catalogue of Stellar Spectral Classification (CSSC; Skiff 2013) was the primary resource used for locating spectral type information, but some of the original sources of spectral types in the CSSC (primarily those pre-dating 1940) could not be tracked down. In those cases, the spectral types are enclosed in parentheses and the provided reference is “C.” Other second-hand spectral types, culled from modern compilations of historical data, are also enclosed in parentheses. The spectral types not enclosed in parentheses are therefore those that could be linked directly to the paper or catalog where the spectral type was determined or estimated.

### 3.3. New Be Star Discoveries

A total of 128 Be stars have been identified as Be stars for the first time via Brackett series emission in APOGEE spectra. According to the BeSS (Neiner et al. 2011), which maintains a comprehensive database of classical Be and main sequence B[e] stars, 2070 Be stars are cataloged in the Milky Way and Magellanic clouds combined. The 128 new Be stars presented in this work therefore represent a  $\sim 6.2\%$  increase in the number of known Be stars.

The positions of all 238 ABE stars are shown in Figure 2, along with the Be star entries included in the BeSS database (Neiner et al. 2011). Although APOGEE observes a large number of fields in the Galactic Halo, the majority (90%) of Be stars observed during the survey reside along the plane of the Milky Way (at Galactic latitudes,  $|b| < 10$ ), similar to the trend seen in BeSS.

Stars included in the ABE sample were generally required to exhibit evidence of emission or shell absorption in at least the H I Br11 line. The exceptions to this rule are ABE-111, ABE-196, and ABE-A06; these stars appear clearly to have emission from Fe II 16878 (see Section 4.2) despite very weak or no emission in the Brackett lines. Figure 3 shows examples of new and previously known Be stars representing the most borderline cases included in the ABE sample. For many of these stars, the Br11 emission is sufficiently weak that double-peaks are not discernible. Rather, the photospheric Br11 absorption wings appear filled in with emission, creating “shoulders” on the line profiles (e.g., ABE-112) and making them easily distinguishable from purely photospheric lines profiles. Fe II emission is also apparent for a number of these stars, despite weakness of the H I emission.

The large number of new Be stars identified by APOGEE is due in large part to the high-resolution, high-S/N spectra which permit identification of very weak disk signatures (e.g., Figure 3) that might be overlooked in lower-resolution spectra or narrow-band photometry. Repeated observations of most of the stars ( $>1$  observation for 93% of sample) can provide confirmation of very weak disk signatures and also reveals transient Be disks, where Brackett series emission either fades away or appears unexpectedly from epoch to epoch (J. P. Wisniewski 2015, in preparation). Among the reasons for 86/128 newly identified ABE stars having been classified in the literature as normal O-, B-, or A-type stars is that the stars did

not possess CS disks at the time the spectral types were determined or estimated.

### 3.4. ABE-144 and ABE-170: the Brightest New Be Stars

The brightest newly identified Be star among the ABE sample is ABE-170, a.k.a. HR 2116 ( $V = 6.36$ ), and the second brightest is ABE-144, a.k.a. HD 189847 ( $V = 6.92$ ). The lack of a prior indicator of emission lines for ABE-144 may be due to few or no historical spectroscopic observations of the star beyond Fehrenbach et al. (1962). It is unclear whether or not Balmer series emission would have been noticed in that study. ABE-170 has been observed spectroscopically in more recent studies including Abt et al. (2002) and Strom et al. (2005), but the spectra used in both of those papers were limited in wavelength coverage to the region encompassing He I 4471 and Mg II 4481, such that emission at H $\alpha$  or H $\beta$  would not have been recognized if present. Among the possible reasons for the Be nature of these stars not having been previously recognized is that ABE-144 and ABE-170 were normal B stars during past observations (similar to, e.g., Bjorkman & Miroshnichenko 2000).

### 3.5. Observed Emission Lines

The emission lines detected in APOGEE’s wavelength range are listed in Table 2. For each line, Table 2 provides the (1) line identification, (2) laboratory rest wavelength, (3) observed wavelength (see concluding paragraph of this section), (4) the difference between laboratory and observed wavelengths, (5) lower level energy  $E_i$ , (6) upper level energy  $E_k$ , (7) transition strength expressed as  $\log(g_i f_{ik})$ , (8) for metallic lines only, the number of confident and possible detections, (9) the number of stars for which  $\Delta v_p$  was measured, (10) the range of  $\Delta v_p$  measurements, (11) the average of all  $\Delta v_p$  measurements, (12) and other transitions possibly contributing to the observed emission line profiles.

Attempts to identify all non-hydrogen (metallic) lines, described in Section 4, made use primarily of Peter van Hoof’s Atomic Line List v2.05b16<sup>14</sup> (PLL from here on) and to a lesser extent the NIST Atomic Database (Kramida et al. 2013) and the Kurucz line list.<sup>15</sup> The identities of metallic emission lines at 15760 and 16781 Å remain ambiguous due to few transitions around the correct wavelengths having available transition probability data needed for confident identification. These lines, referred to as  $\lambda 15760$  and  $\lambda 16781$  throughout this paper, are discussed in more detail in Section 4.5. Since forbidden line emission was present for only one source, ABE-A23 a.k.a. MWC 922, the central star of the Red Square Nebula (Tuthill & Lloyd 2007), Table 2 is limited to the permitted (E1) transitions observed for Be stars. The  $H$ -band spectrum of MWC 922 is sufficiently different from the rest of the sample and sufficiently more complex that an in-depth analysis is currently being pursued separately (Whelan, in preparation).

The observed wavelengths as well as the differences between laboratory and observed wavelengths, provided in columns (4) and (5) of Table 2, pertain to the average position of double emission peaks for each line plus a correction factor based on

<sup>14</sup> <http://www.pa.uky.edu/~peter/newpage/>

<sup>15</sup> 1995 Atomic Line Data (R.L. Kurucz and B. Bell) Kurucz CD-ROM No. 23. Cambridge, MA: Smithsonian Astrophysical Observatory.

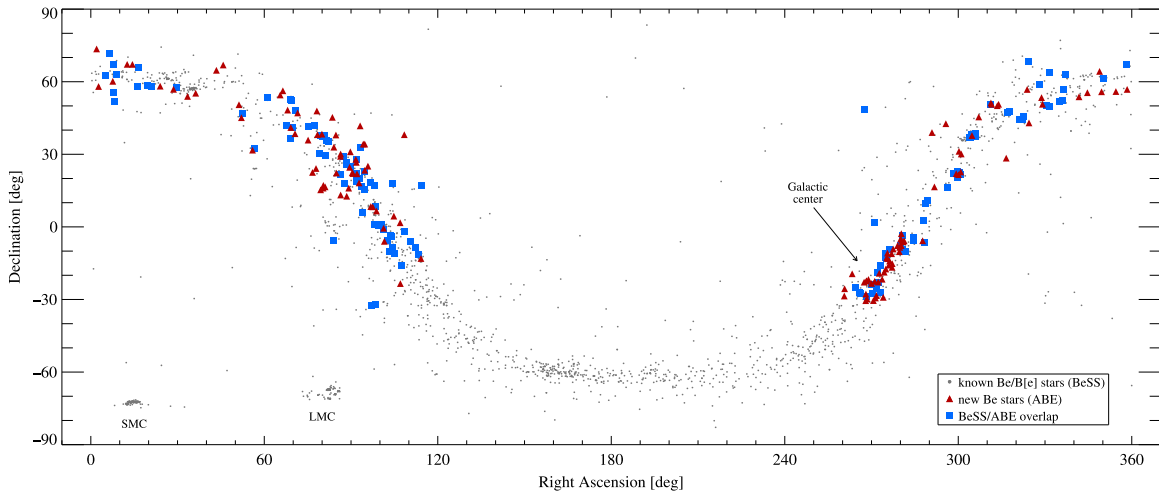


**Figure 2.** This adaptation of Neiner et al. (2011) Figure 1 shows the RA and decl. positions of all the BeSS entries as black dots, known Be stars observed by APOGEE as squares (blue), and new Be stars discovered in the APOGEE survey as triangles (red). The Galactic Center and Magellanic Clouds are labeled.

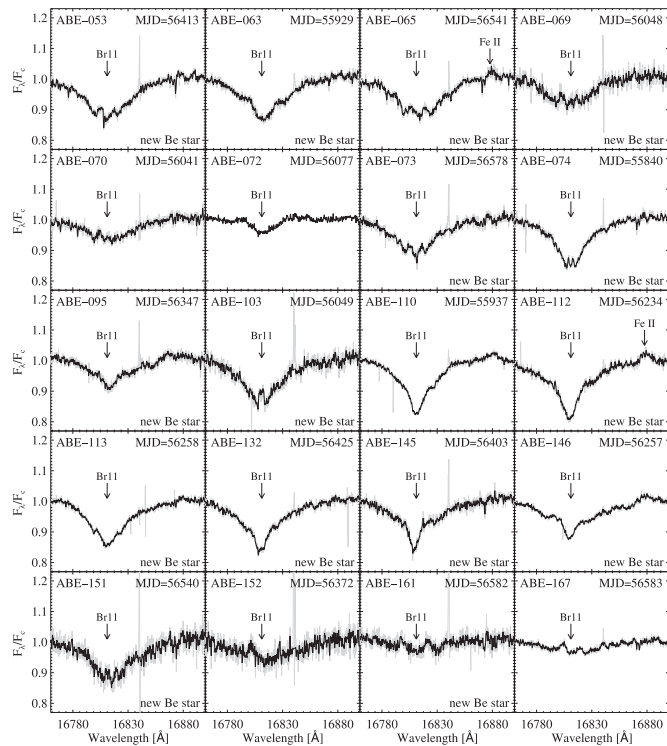


**Figure 3.** Br11 region for some new and previously known Be stars showing very weak evidence of circumstellar emission.

the Doppler shift found for the Br11 line. Br11 is the strongest line covered for these stars and provides the most reliable peak position measurements, so correction to rest frame was done simply by adding to the observed wavelength of each line the difference between Br11 emission peak midpoint and Br11 rest wavelength.

## 4. NON-HYDROGEN LINE IDENTIFICATION

### 4.1. Diffuse Interstellar Bands

The DIB at 15271 Å, discovered by Geballe et al. (2011), is present in most of the ABE spectra and in numerous

APOGEE spectra (Zasowski et al. 2014). Because DIB 15271 usually falls on or near the Br19 R emission peak, Br19 peak separation measurements are omitted from this paper. Examples of DIB 15271 absorption (marked with red dotted lines) in spectra for four active Be stars and two currently emission-less stars are displayed in Figure 4. Other DIBs (15615, 15651, 15671 Å) discussed in Geballe et al. (2011) are present for most objects with DIB 15271, as are other possible DIBs at  $\sim 15314$  and  $\sim 16154$  Å. Of the spectra shown in Figure 4, DIB 15314 appears most prominently in the spectrum for ABE-137.

### 4.2. Fe II

The Fe II 16878 line appears in emission for between 32%–46% (upper limit includes weak or ambiguous detections) of the 238 active Be stars discussed here, making it the most frequently observed metallic feature in APOGEE’s coverage of the *H* band. For stars with very strong Fe II 16878, the much weaker Fe II 16792 also appears in emission but is usually blended with Br11. As for Fe II 16878, proximity of the feature to C I 16895 often leads to a blend of the two lines, especially since C I emission is always broad compared to Fe II (see Section 5.2).

Examples of stars with emission from one or both *H*-band Fe II lines are presented in Figure 5. The left panel demonstrates the wide range of H I strength corresponding to Fe II detections. As is seen quite clearly for the lowermost stars (ABE-A06, ABE-111) in the left panel of Figure 5, Fe II emission may be present even when there is no perceptible emission from Brackett series lines, contrary to the finding of Steele & Clark (2001). ABE-A06 has been a Be-shell star at various epochs (see BeSS spectra), but in the APOGEE data exhibits only very weak filling of the Br11 photospheric absorption wings in addition to the weak Fe II 16878 emission that, for ABE-A06, persists in four spectra sparsely covering 0.77 years. Less evidence is available for H I emission in the case of ABE-111, despite the Fe II feature appearing in all six APOGEE covering 2.29 years. Though not shown in Figure 5, ABE-196 also lacks convincing evidence of H I emission and yet exhibits Fe II 16878 emission in all 13 APOGEE spectra covering 3.02 years. Line profile variability in the Brackett lines is observed for all

**Table 2**  
Observed Emission Lines and Summary of  $\Delta v_p$  Measurements

(1)	(2)	(3)	(4)	(5)	(6)	(7)	(8)	(9)	(10)	(11)	(12)
Atom or Ion	$\lambda_{vac}$ lab (Å)	$\lambda_{vac}$ obs <sup>a</sup> (Å)	Diff. lab–obs (Å)	$E_i$ (eV)	$E_k$ (eV)	$\log(gf)$	N detections yes (maybe)	$\Delta v_p$ N stars	$\Delta v_p$ range (km s <sup>-1</sup> )	$\Delta v_p$ mean (km s <sup>-1</sup> )	Other possible contribution
H I (Br20)	15195.996	15195.932	0.064	12.749	13.564	-1.487	...	48	68–566	314	...
H I (Br19)	15264.708	...	...	12.749	13.561	-1.414	...	...	...	...	DIB 15271
Fe I	15298.740	15298.528	0.212	5.309	6.119	0.650	6	3	188–283	228	...
H I (Br18)	15345.982	15345.987	-0.005	12.749	13.556	-1.337	...	57	67–533	276	...
H I (Br17)	15443.139	15443.187	-0.048	12.749	13.551	-1.255	...	73	66–537	266	...
H I (Br16)	15560.699	15560.697	0.002	12.749	13.545	-1.166	...	47	65–436	266	...
N I	15586.545	15586.591	-0.046	12.126	12.922	-0.023	1	1	52–52	52	...
H I (Br15)	15704.952	15705.015	-0.063	12.749	13.538	-1.071	...	76	65–552	282	...
Mg I	15753.291	blend	...	5.932	6.719	0.140	7	...	...	...	Mg I 15745
$\lambda$ 15760	...	15760.161	...	...	...	...	36 (13)	11	27–304	161	Mg I
Mg I	15770.149	15770.943	-0.794	5.933	6.719	0.411	9 (1)	2	338–375	356	$\lambda$ 15760
H I (Br14)	15884.880	15884.875	0.005	12.749	13.529	-0.967	...	91	61–522	259	...
Si I	15892.771	blend	...	5.082	5.862	-0.007	6	...	...	...	...
Si I	15964.422	15963.229	1.193	5.984	6.761	0.198	7 (1)	3	321–383	345	...
C I	16009.270	blend	...	9.631	10.406	0.234	7 (3)	...	...	...	...
C I	16026.080	blend	...	9.631	10.405	0.222	5 (5)	...	...	...	...
H I (Br13)	16113.714	16113.766	-0.052	12.749	13.518	-0.852	...	96	61–517	249	...
H I (Br12)	16411.674	16411.763	-0.089	12.749	13.504	-0.725	...	95	59–524	252	...
Ca II	16565.590	16565.973	-0.383	9.235	9.983	0.368	6	3	208–333	291	C I 16564
Ca II	16654.430	blend	...	9.240	9.984	0.626	1 (2)	...	...	...	...
Si I	16685.341	blend	...	5.984	6.727	-0.117	1 (2)	...	...	...	...
Mg II	16764.800	16764.922	-0.122	12.083	12.822	0.481	2 (2)	1	34–34	34	...
$\lambda$ 16781	...	16781.115	...	...	...	...	36 (13)	13	28–309	157	...
Fe II	16791.762	16791.953	-0.191	5.484	6.222	-2.325	8 (6)	1	48–48	48	...
Mg II	16804.520	blend	...	12.085	12.822	0.737	2 (2)	...	...	...	Mg II 16804
H I (Br11)	16811.111	...	...	12.749	13.486	-0.582	...	194	57–1153	282	...
Fe II	16877.808	16877.822	-0.014	5.484	6.219	-1.256	76 (33)	26	24–232	82	...
C I	16895.031	16894.898	0.133	9.003	9.736	0.534	43 (19)	14	31–539	243	...
Si II	16911.430	16911.646	-0.216	12.147	12.880	0.350	1 (1)	1	41–41	41	...

<sup>a</sup> The emission peak midpoint corrected by the emission peak midpoint of Br11.

three stars and is likely due to varying degrees of emission filling, but lack of knowledge of the true photospheric absorption profiles prevents us from confidently claiming H I emission is present.

The right panel of Figure 5 focuses on some of the more extreme Be stars in this sample, starting with the obvious outlier ABE-A23, an unclassified B[e] star (Lamers et al. 1998) for which the exceptionally strong Fe II and [Fe II] emission lines reported by Rudy et al. (1992) dominate the APOGEE spectra. In contrast to ABE-A23, where the emission lines all appear truly single-peaked, ABE-137 is likely a classical Be star viewed at an inclination,  $i$ , of nearly or exactly zero. The Brackett series lines for ABE-137 show some peak structure even though the peaks are not resolved. The Fe II 16878 line is very narrow and pointed but double peaks are resolved in the C I 16895 line, suggesting the presence of a circumstellar disk. ABE-A35 exhibits strong Fe II emission, and is the only source of the ABE sample for which the  $\Delta v_p$  of Fe II 16792 could be measured. The average Fe II peak separations from five spectra for ABE-A35 are in good agreement:  $\Delta v_p(\text{Fe II } 16878) = 52.6 \pm 2.53 \text{ km s}^{-1}$ ,  $\Delta v_p(\text{Fe II } 16792) = 48.3 \pm 4.01 \text{ km s}^{-1}$ . The lower resolution of red detector data from APOGEE commissioning data is likely a factor in the single-peaked appearance of the Fe II lines for ABE-015.

### 4.3. Fe II Profiles as a Function of Inclination

In past studies, optical Fe II lines have been used (Hanuschik 1996) to establish a strict definition of the shell, or edge-on, class of Be stars. Photospheric Fe II absorption lines are usually observed at greatest strength for A–F supergiants (Gray & Corbally 2009), so if the central depression of an Fe II emission line for a Be star extends below undisturbed, adjacent continuum level, the implication is that the the disk is viewed at sufficiently large inclination that our line of sight passes through an appreciable volume of cool gas in the inner, equatorial disk. It is a well-known fact that Fe II and Ti II shell lines are among the strongest metallic features present in the spectra of edge-on Be stars.

In contrast to the observed behavior of optical Fe II lines, stars with obvious shell absorption in the Brackett series lines exhibit no evidence of shell absorption in the  $H$ -band Fe II lines nor in any of the covered metallic lines, such that the Fe II line profile shapes for pole-on Be stars differ from those of edge-on Be stars only in line width. This fact is demonstrated in Figure 6, where the upper panel compares Br11 and Fe II profiles for five stars viewed over a range of inclination angles. As can be seen, the Fe II profiles are pure emission regardless of the what form the H I profiles take. The lower right panel of Figure 6 presents additional examples of H I-shell stars with

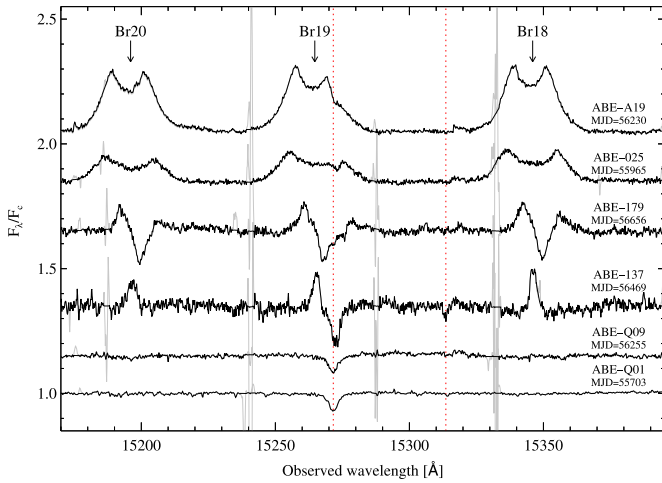


**Figure 4.** Spectra for six stars with visible DIB 15271 absorption around or on the Br19 line. No correction for radial velocity has been applied to the spectra. The dotted lines (red) mark DIB 15271 and another likely DIB at  $\sim 15314$  that appears in numerous APOGEE spectra.

Fe II emission, while the lower left panel (as well as the edge-on example in the upper panel) highlights ABE-035, the most extreme shell star within this sample in terms of Brackett series shell depth.

#### 4.4. C I and Other Neutral Lines

An emission line at 16895 Å is identified for the first time as C I 16895.031 and is observed for between 18–26% of the 238 Be stars. Figure 5 displays 11 examples of stars with C I emission and the strongest detections will be discussed in Section 4.4.1. A C I 16895 absorption line is present in numerous APOGEE spectra of A–F stars, but the line is typically not present for OB stars unless in emission. Except in the case of very narrow-lined Be stars (e.g., ABE-015, ABE-040 in Figure 5), the R peak of the C I 16895 emission profile is frequently compromised by a strong airglow line around  $\sim 16904$  Å.

Prior mentions in the literature of NIR C I emission include Groh et al. (2007) and Štefl et al. (2009), where several C I emission lines were detected around 10700 Å in Be star spectra. Spectra showing C I 16895 emission have been included in a number of papers, but the line is usually either confused and/or blended with Fe II 16878, or not identified at all. Ashok & Banerjee (2000) noticed the C I 16895 line in a subset of low-resolution Be star spectra and realized that it was probably not Fe II 16878 due to the measured wavelength of the line ( $\sim 16893$  Å, or  $\sim 15$  Å from the Fe II wavelength). Kendall et al. (2003) presented medium resolution *H*-band spectra of three young stellar object (YSO) candidates, one of which, IRAS 17441–2910, was found to be a very strong emission line source. A plot of the spectrum shows single-peaked Br11 and Fe II 16878 emission and strong double-peaked C I 16895 emission, but the authors did not comment on the latter.

NIR emission from C I is not limited to classical Be stars. C I 16895 emission was present in a high-resolution spectrum shown by Kraus et al. (2012) for the Herbig B[e] star V921 Scorpii, and the C I emission line is also present in APOGEE spectra for both B[e] stars observed by APOGEE to date (see right-hand panel of Figure 5). Even luminous blue variable stars display evidence of C I emission lines (Groh et al. 2007),

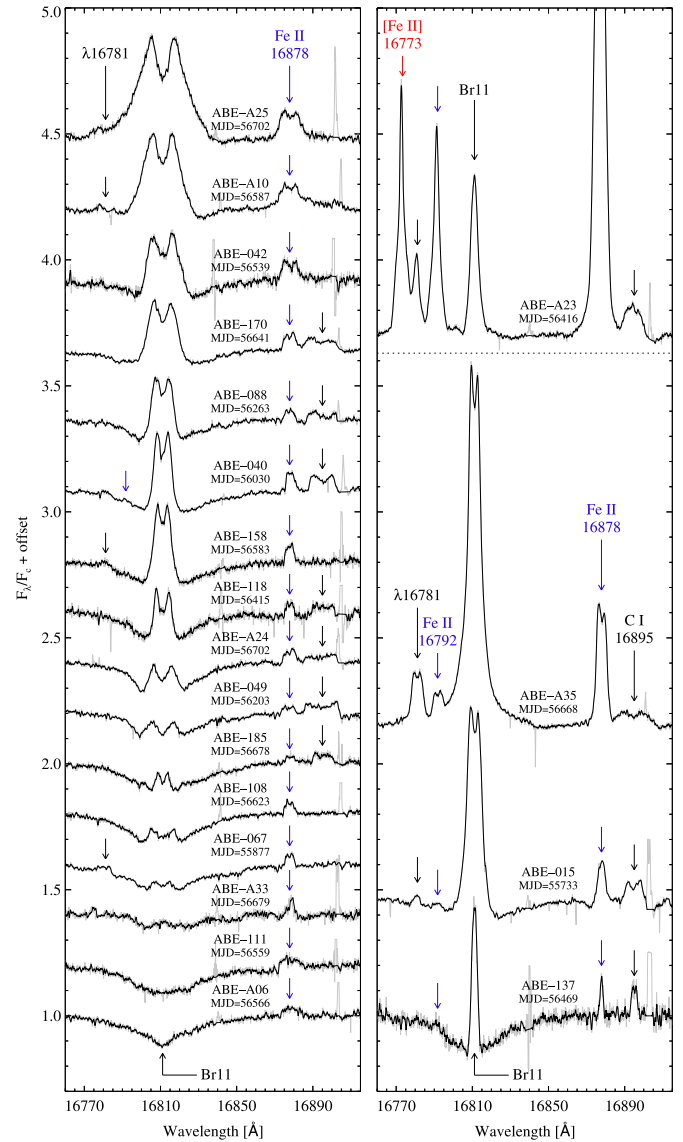


**Figure 5.** Be star spectra with combinations of emission from  $\lambda 16781$ , Fe II 16792 and 16878 (blue), and C I 16895 over a spectrum of Brackett series emission strength. The left and right panels show the same wavelength and intensity ranges. A dotted line separates the unclassified B[e] star ABE-A23 (MWC 922) from the other stars; ABE-A23 is unique among this sample (see Section 3.5) in being the only source to show forbidden line emission (mostly [Fe II]).

suggesting that NIR C I emission is ubiquitous across a wide range of evolutionary states.

##### 4.4.1. C I-strong Be Stars

Abnormally strong C I 16895 emission is accompanied by weaker, similarly profiled emission lines from neutral and singly-ionized species in the spectra for at least five ABE stars. Figure 7 displays full APOGEE spectra for ABE-A15, ABE-188, and ABE-084, ABE-031, and ABE-004, the best examples of this marked deviation from the typical *H*-band emission line content for Be stars. The C I 16895 emission is blended with Fe II 16878 for ABE-A15 and possibly also for ABE-188. Two other C I lines at 16009.27 Å and 16026.08 Å are blended in emission for these stars, leading us to refer to the group as “C I-strong” Be stars.

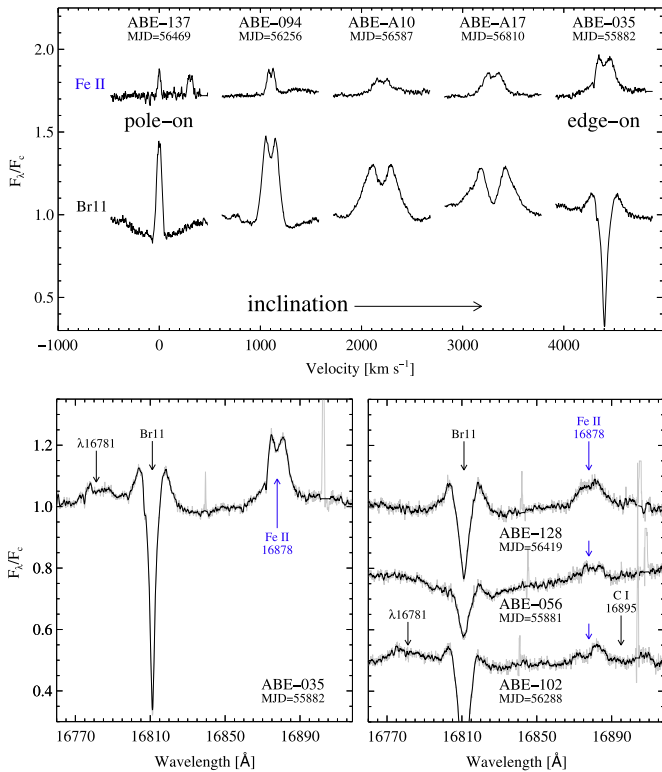


**Figure 6.** (Top panel) An assortment of observed spectra, showing the variety of metallic and hydrogen line profiles observed in the sample as a function of inclination angle. (Left, bottom) A portion of a spectrum for ABE-035, highlighting the immunity of metallic emission lines to shell absorption, a fact that is observed in all shell absorption sources (examples shown on right, bottom).

Most of the metallic emission features for the C I-strong Be stars correspond to strong absorption lines for late-A and cooler stars. An APOGEE spectrum for HD 163271, which is either a single metallic-line A star (A2/A3m) or the superposition (A2/A3+F0) of an A star with an F star (Houk & Smith-Moore 1988; Renson et al. 1991), is provided in Figure 7 to demonstrate the typical line content for A–F stars. Small blue line segments indicate the numerous strong Fe I lines covered, with Fe I 15299 being the strongest and appearing in emission for the Be stars. It is likely that emission from other Fe I lines is involved in much of the blending in the C I-strong Be star spectra.

Detections of resolved emission peaks for the S I lines labeled in Figure 7 are unavailable, but the lines may contribute to the weak bumps and blending around Br17. The transition probability measures for these S I lines suggests S I 15426 should be the strongest of them and the A star spectrum appears to confirm this. Since the Br17 profiles for the C I-strong Be stars do not appear distorted by significant underlying emission from other lines however, it is unclear whether the S I lines are actually observed as emission features.

The strong emission lines redward of Br15 are due partly to several Mg I lines, with the strongest contributions being Mg I 15753.291 and Mg I 15770.149. The Mg I lines are also seen weakly in emission and unblended for ABE-149; all of the emission lines are single-peaked for that source, including H I, Fe II 16878, C I 16895, and the Mg I lines (see the Appendix). Above the ABE-A15 spectrum in Figure 7 is a small panel that zooms in on the Mg I blend for ABE-A15,

demonstrating that emission from  $\lambda 15760$  is also a major contributing factor in the blend. Black arrows in the small panel point out the sharp  $\lambda 15760$  peaks that mimic the sharp  $\lambda 16781$  peaks. ABE-004 similarly has the  $\lambda 15760$  and  $\lambda 16781$  lines clearly in emission.

As for the line around 15964 Å, PLL suggests two possible identities: C I 15964.11 and Si I 15964.4218. Since other covered C I lines are expected to be stronger than C I 15964.11 are covered but do not appear in emission (e.g., C I 15524.70), Si I seems the more likely to cause the 15964 Å emission. The line blended with Br14 (most noticeable for ABE-084 and ABE-031) is suspected to be Si I 15892.7713, the next strongest Si I line covered after Si I 15964.4218.

The weak double-peaked line around  $\sim 16565$  Å is possibly Ca II 16565.59, but the ambiguous detection of Ca II 16654.43 calls the Ca II identification into question since the latter line should be stronger. On the other hand, the position of Ca II 16654.43 corresponds to a strong telluric band which is poorly corrected and may cause the ambiguity. Emission from the Ca II triplet (8498, 8542, 8662 Å) is observed for some Be stars (Hiltner 1947; Polidan & Peters 1976), so H-band Ca II emission would not be terribly unexpected. A C I line at 16564.13 Å probably does not contribute since similar C I lines, covered and expected to be stronger than C I 16564, fail to appear.

The cause of the strong C I 16895 in addition to other weaker emission lines for the C I-strong Be stars remains unknown. Based on the available examples however, such as ABE-031 where the weak emission features persist in 12 spectra covering 1.2 years, the phenomenon appears to be permanent rather than a particular stage of short- or medium-term intrinsic variability.

#### 4.5. $\lambda 15760$ and $\lambda 16781$

The  $\lambda 15760$  and  $\lambda 16781$  emission lines discussed by Steele & Clark (2001) are present for between 15–21%. As is demonstrated in Figure 8, these lines always appear together with matching intensity and V/R orientation. In the available examples where peak separations were measurable for  $\lambda 15760$  and  $\lambda 16781$ , those values are nearly identical as well (see Section 5.2). Fe II 16878 is usually detected in unison with  $\lambda 15760$  and  $\lambda 16781$ , but this is not a strict rule. Non-detection of Fe II 16878 is accompanied by detections  $\lambda 15760$  and  $\lambda 16781$  for ABE-180, ABE-A05, and ABE-005, the three lower-most stars represented in Figure 8.

The  $\lambda 15760$  line has been identified as Fe II in several past papers (Steele & Clark 2001; Smith 2001; Kraus et al. 2012). In a study of  $\eta$  Carinae, Hamann et al. (1994) was apparently the first to note proximity of  $\lambda 15760$  to an Fe II transition. The authors of that paper appended a question mark to the Fe II identification listed in an emission line table, but it seems that over the years the question mark was forgotten. PLL lists an Fe II line at 15761.78 Å, but no indication of expected transition strength is available. NIST provides wavelength for different Fe II transitions, at 15759.720 and 15760.563 Å, with the lower energy levels again more than doubling those of Fe II 16878 (5.5 eV versus 13.4 eV) and again lacking transition strength indication. A firm identification for this emission line remains elusive.

Whereas Steele & Clark (2001) restricted the possible identifications for  $\lambda 16781$  to [Fe II] 16773 and Fe II 16792, the much higher-resolution APOGEE spectra rule out both of

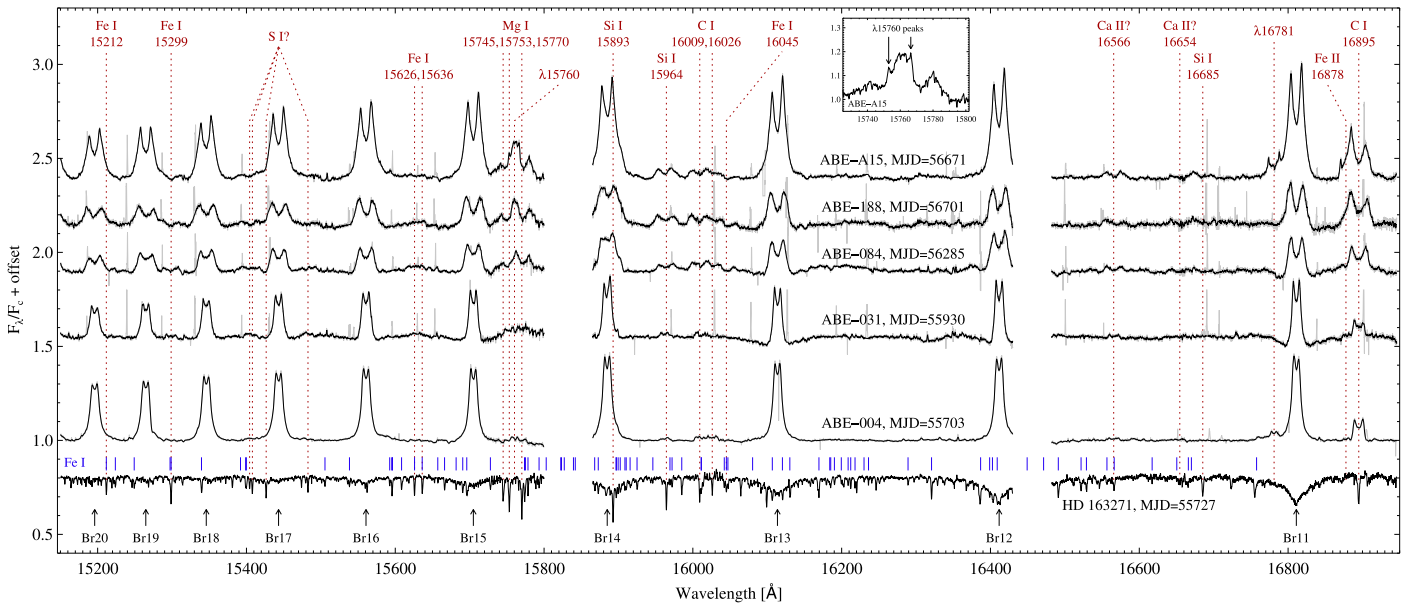


**Figure 7.** Spectra of five Be stars (ABE-A15, ABE-188, ABE-084, ABE-031, ABE-004) with strong C I 16895 emission and many weak, double-peaked metallic emission features. The spectrum of a strong-metal-lined A star (HD 163271) is included to demonstrate that the additional emission lines for these four Be stars correspond to absorption lines for cooler stars. The small lines (blue) above the A star spectrum mark the positions of numerous Fe I lines with  $\log(g_f/i_k) > -3$ .

those lines as possibilities (see ABE-A23 spectrum in Figure 5). PLL includes several He I lines around 16780 Å, but considering that an absorption line is never seen at this wavelength for normal OB stars,  $\lambda 16781$  is probably not He I. Also listed in PLL is an O I multiplet at 16781.7 Å, lacking transition probability data and being quickly ruled out by non-detection of other O I lines covered and expected to be stronger. Through similar argument, other lines listed in PLL and NIST around  $\lambda 16781$  are readily ruled out as possibilities.

Whatever the identities of  $\lambda 15760$  and  $\lambda 16781$ , the features behave similarly to Fe II in being present as emission lines or not present at all: no corresponding absorption for features are seen for APOGEE-observed stars of any type. Reliable spectral types have been reported for 24 ABE stars with  $\lambda 15760$  and  $\lambda 16781$  detections and 20/24 are B3 or hotter, so it is possible that  $\lambda 15760$  and  $\lambda 16781$  are relatively high-ionization lines. One possible example of  $\lambda 16781$  being detected despite absence of  $\lambda 15760$  is ABE-A36, a peculiar star discussed in Section 6.1. However, the bump in the V wing of Br11 for ABE-A36 is not sufficiently convincing to cause us to doubt that  $\lambda 15760$  and  $\lambda 16781$  should always be expected to appear simultaneously.

#### 4.6. N I

The expected strongest and second strongest N I lines covered are seen in emission for ABE-A35. Figure 9 shows a portion of a spectrum for ABE-A35 encompassing the N I 15586.545 and N I 15687.160 lines as well as Br16, Br15 and  $\lambda 15760$ . Neither of the N I lines are detected for any other objects beyond ABE-A35, but they are present in all five APOGEE spectra for ABE-A35. Although [Fe II] 15586.550 is coincident in position with the stronger N I line, it is far from the strongest [Fe II] feature covered. The lack of detection in the ABE-A35 spectra of the stronger [Fe II] lines rules those lines out as possibilities. Forbidden line emission in the optical was noted as early as 1976 for ABE-A35 (Allen & Swings 1976),

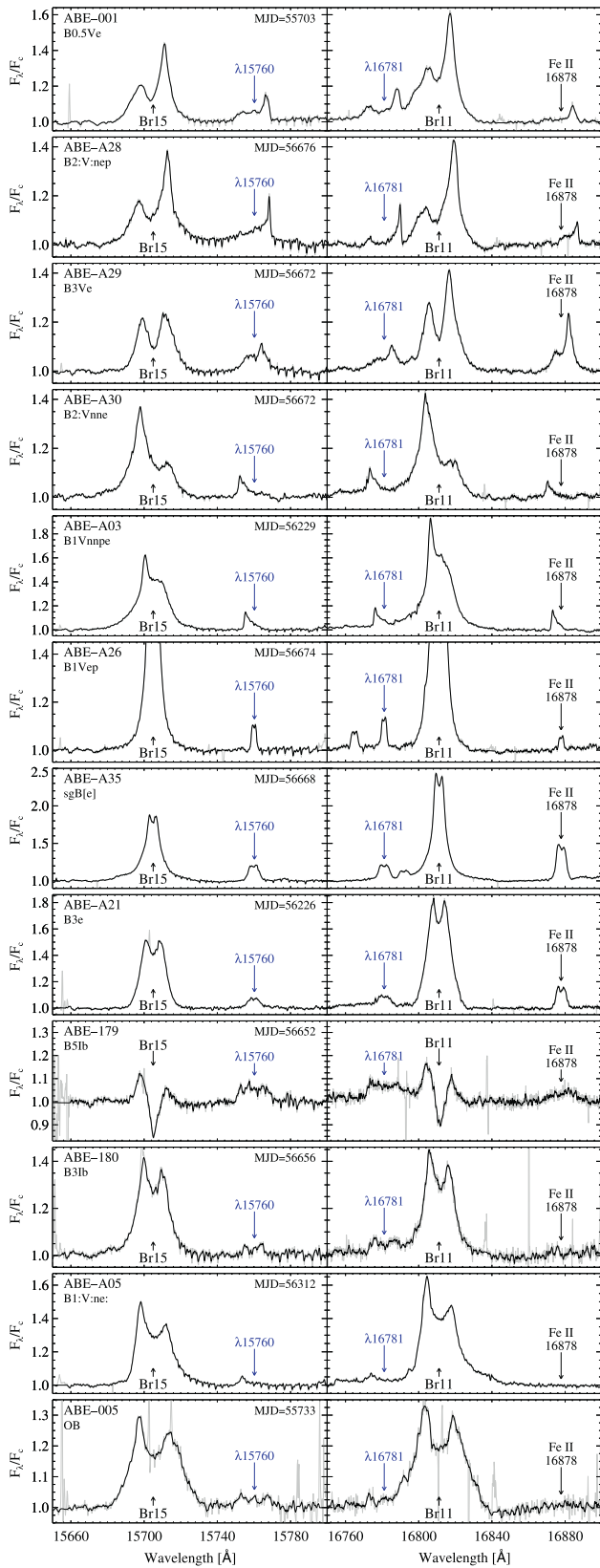
but in the *H*-band the only clues suggesting the B[e] nature of this object are the abnormally strong H I, Fe II, and Fe II-like emission lines.

#### 4.7. Mg II and Si II

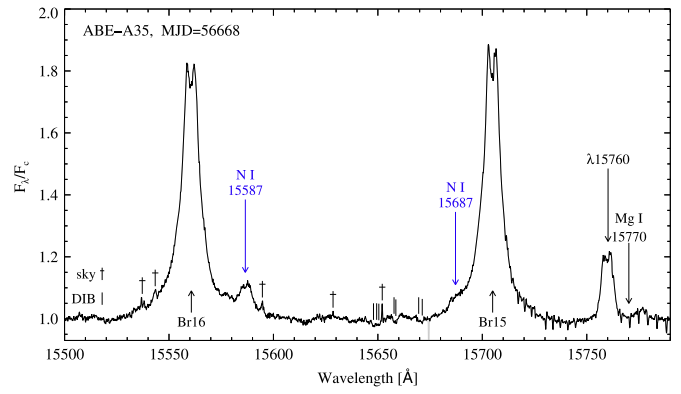
The lowest-energy Mg II and Si II lines covered in APOGEE data appear clearly in emission for ABE-A26 and are not confidently detected for any of the other stars. ABE-004, ABE-A05, and ABE-A29 possibly show exceedingly weak contributions from these lines, but blending renders the situation ambiguous in all cases aside from ABE-A26.

Figure 10 displays a spectrum for ABE-A26 over differing wavelength ranges: the upper panel shows the full spectrum, while the middle and lower panels focus on the weak emission lines around Br11. Identification of the line blueward of  $\lambda 16781$  as Mg II 16764.80 requires that the stronger of three lines comprising this Mg II multiplet also be detected, and indeed the lower panel of Figure 10 shows that Mg II 16804.52 is visible in the V wing of Br11 at apparently the correct intensity relative to Mg II 16764.80. Based on the intensities of these lines, the third Mg II line of the multiplet (16803.67 Å) is not expected to appear and would overlap with Mg II 16804 anyway. The weak emission line redward of Fe II 16878 in the middle panel of Figure 10 is identified as Si II 16911.430, the strongest Si II line covered and a line with very similar energy levels to the Mg II lines (see Table 2).

In addition to detection of the relatively high-ionization Mg II and Si II lines, the combination of single-peaked Brackett series lines and double-peaked metallic lines is unique to ABE-A26 among this sample. The double-peaked lines indicate that at least some of the circumstellar gas is organized in a disk. It is possible that ABE-A26 was observed by APOGEE during of after an outburst such that substantial Brackett series emitting gas is in the polar regions, leading to the single-peaked Brackett lines.



**Figure 8.** Identifications of  $\lambda 15760$  and  $\lambda 16781$  are uncertain; however, these lines are never detected separately and in most cases Fe II 16878 emission is also present. The three lines always share a common V/R orientation, but the Fe II intensity varies with respect to  $\lambda 15760$  and  $\lambda 16781$ . Small absorptions around the  $\lambda 15760$  line are telluric correction artifacts.



**Figure 9.** Emission from N I is seen only for ABE-A35, a supergiant B[e] star (Esteban & Fernandez 1998; Oksala et al. 2013). Both lines, N I 15587 and N I 15687, are partially blended with H I emission wings.

## 5. PEAK SEPARATIONS

### 5.1. Stars with Abnormally Large $\Delta v_p$

Optical spectroscopy revealed that two stars, ABE-050 (HD 345439) and ABE-075 (HD 23478), with extremely large Brackett emission widths and double-peak separations are not classical Be stars (Eikenberry et al. 2014). Rather, these stars are analogues to the prototype magnetic emission B star  $\sigma$  Orionis E first described as “helium-rich” by Greenstein & Wallerstein (1958) and subsequently providing the first application (Townsend et al. 2005) of the Rigidly Rotating Magnetosphere model of Townsend & Owocki (2005). Large  $\Delta v_p$  for the Brackett series emission was a clue suggestive of a non-classical nature for these stars, but confirmation lay in the fact that both stars exhibit H I emission well beyond the projected  $v \sin i$  values (in these cases, a factor of two or more beyond the projected  $v \sin i$ ). For classical Be stars with Keplerian disks, the velocity separations of emission peaks do not exceed  $2 v \sin i$  (Dachs et al. 1992).

Figure 11 compares the Br11 profiles of ABE-050 and ABE-075 to the stars with the next largest peak separations. Arrows indicate the measured peak separations and for ABE-050 and ABE-075, the inner sets of arrows indicate the  $v \sin i$  values from Eikenberry et al. (2014). As there are only a handful of magnetic B emission stars known to exist, it seems more likely that the ABE-155, ABE-168, ABE-124, and ABE-099 are weak-disked, edge-on classical Be stars rather than additional  $\sigma$  Orionis E types. Either way, optical follow-up spectroscopy is required for proper diagnosis.

### 5.2. Line-by-line $\Delta v_p$ Comparison

Figure 12 plots the peak separations for Br11 versus the peak separations for Br12–Br18, Br20,  $\lambda 16781$ ,  $\lambda 15760$ , Fe II 16878, Fe II 16792, C I 16895, Si I 15964, and Mg I 15770. Each point represents the average peak separation for a line, from all spectra for a given star in which the Br11  $\Delta v_p$  was measured in addition to the  $\Delta v_p$  of the line represented on the y-axis. In the upper nine panels, plus signs (red) correspond to stars for which the Br20 peak separation was measured and therefore to stars with strong or particularly sharp-peaked emission. The

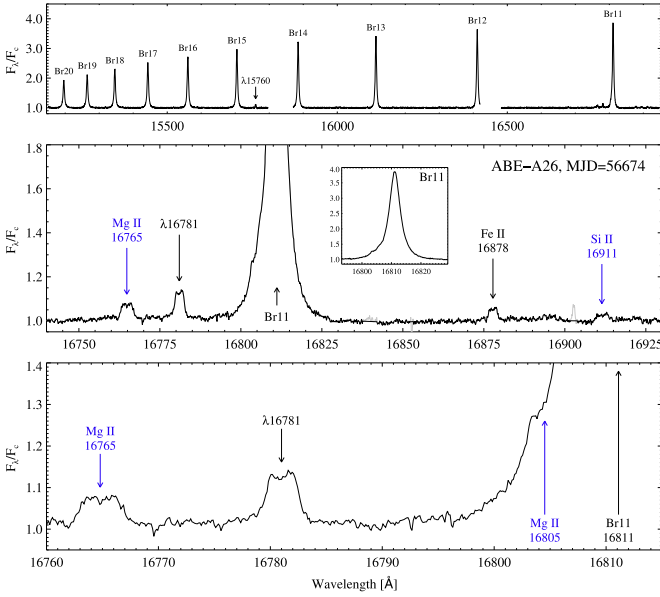


**Figure 10.** Mg II and Si II emission lines in a spectrum of ABE-A26, the only star for which these lines are detected. While the full spectrum is presented in the upper panel, the lower two panels highlight the Br11 region and the weak metallic lines therein. The single-peaked Br11 line profile is displayed in the inset panel of the larger middle panel for comparison to the double-peaked profiles of the metallic lines. As expected from the detection of Mg II 16765, the stronger line of this multiplet, Mg II 16804, appears blended with Br11 in the lowermost panel.

gaps between  $\sim 400$ – $500 \text{ km s}^{-1}$  in the Br11 versus Br18 and Br11 versus Br17 panels are due to strong airglow lines impacting the emission peaks at large line width. High velocity gaps in the Br11 versus Br12 and Br11 versus Br14 panels are caused by either the Br12 V peak or the Br14 R peak falling too close to gaps between detectors. For Br13 and Br15, telluric absorption contamination is more likely for large line width. Grey lines indicate 1-to-1 relationships between the lines plotted in each panel.

The effect of increasing  $\Delta v_p$  toward weaker H I lines is well-known for the Balmer (Hanuschik et al. 1988) and Paschen (Andrillat et al. 1990) lines, and the Brackett series lines are not an exception. Some stars (primarily the narrow-lined variety with Br11  $\Delta v_p < 200 \text{ km s}^{-1}$ ) show very little or no variation among Brackett series  $\Delta v_p$  but no convincing examples are found of decreasing  $\Delta v_p$  from Br11 toward Br20. We interpret the increasing peak separations toward weaker lines as kinematic in nature, such that the weaker Brackett lines (Br12–20) are simply formed closer to the rapidly-rotating central stars than e.g., Br11. The Br11–20 lines never take the form of winebottle-type profiles frequently observed in the optically thick H $\alpha$  line, where the effect of non-coherent scattering can produce inflections in the emission profile and effectively reduce the observed peak separation (Hummel & Dachs 1992). Section 4 of Hanuschik et al. (1996) provides a summary of the line broadening factors that contribute to Be star emission line profile shapes.

Based on the lower three panels of Figure 12, when the  $\Delta v_p$  of  $\lambda 15760$  and  $\lambda 16781$  are measured simultaneously, very similar values are found. The  $\Delta v_p$  for these lines are usually slightly smaller than the Br11  $\Delta v_p$  but can be slightly larger as

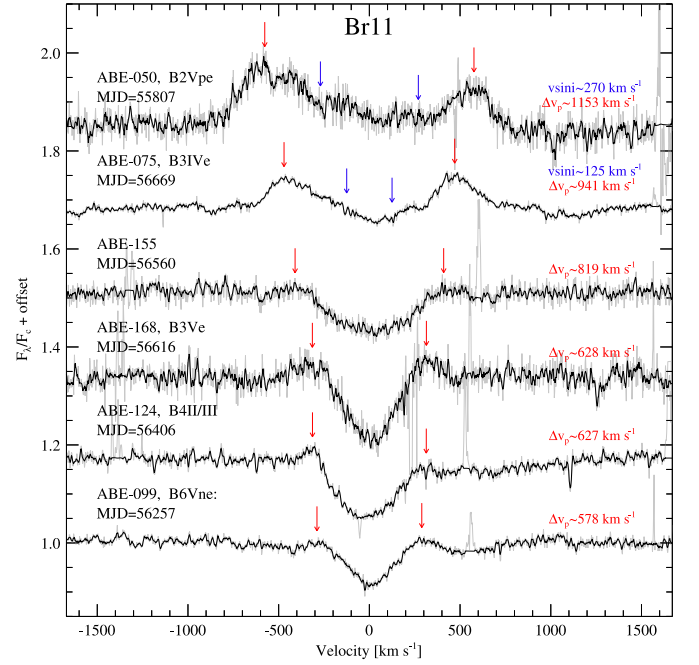


**Figure 11.** Br11 line profiles for the ABE stars with the largest peak separations are shown. The  $\Delta v_p$  is listed and marked with arrows (red) for each source, while the  $v \sin i$  measurements for ABE-050 and ABE-075 are given and indicated with arrows (blue) interior to the  $\Delta v_p$  arrows. Whereas ABE-050 and ABE-075 are confirmed  $\sigma$  Orionis E type stars, the other four stars remain to be investigated further.

well. Excluding ABE-A26, for which Br11 is single-peaked, Fe II 16878 is a strictly small- $\Delta v_p$  line relative to Br11 with all  $\Delta v_p$  measurements less than  $140 \text{ km s}^{-1}$ . The C I 16895 Si I 15964, and Mg I 15770 lines share nearly identical  $\Delta v_p$  in the available examples (ABE-084, ABE-188, ABE-A15; see Figure 7), and all of the  $\Delta v_p$  measurements for C I 16895 exceed the Br11  $\Delta v_p$ .

### 5.3. Line-emitting Disk Radii

For Keplerian rotation in a gaseous disk, the orbital velocity decreases according to  $r^{-1/2}$ , where  $r$  is the radial distance from star to disk. Given knowledge of the stellar rotational velocity,  $v \sin i$ , the peak separation of an emission line in the disk,  $r_d$ , at which that line is preferentially formed (Smak 1969; Huang 1972; Smak 1981; Horne & Marsh 1986). Many authors (e.g., Hanuschik 1987; Hanuschik et al. 1988; Andrillat et al. 1990; Dachs et al. 1992; Slettebak et al. 1992) have used this relation (Huang’s law) to study the geometry of Be disks by estimating the individual line-emitting radii for H I and metallic lines in the optical region. In units of stellar radii,  $R_*$ ,  $r_d$  is calculated via Huang’s Law (Huang 1972) as

$$r_d = \left( \frac{2 \times v \sin i}{\Delta v_p} \right)^2 \quad (1)$$

where the Equation is squared due to the assumption of a circular orbit. The resulting outer disk radii measurements for the subset of stars with available  $v \sin i$  from the literature and Br11 or metallic line  $\Delta v_p$  measurements are listed in Table 3. In estimating  $r_d$ , the average  $\Delta v_p$  measured from all spectra for

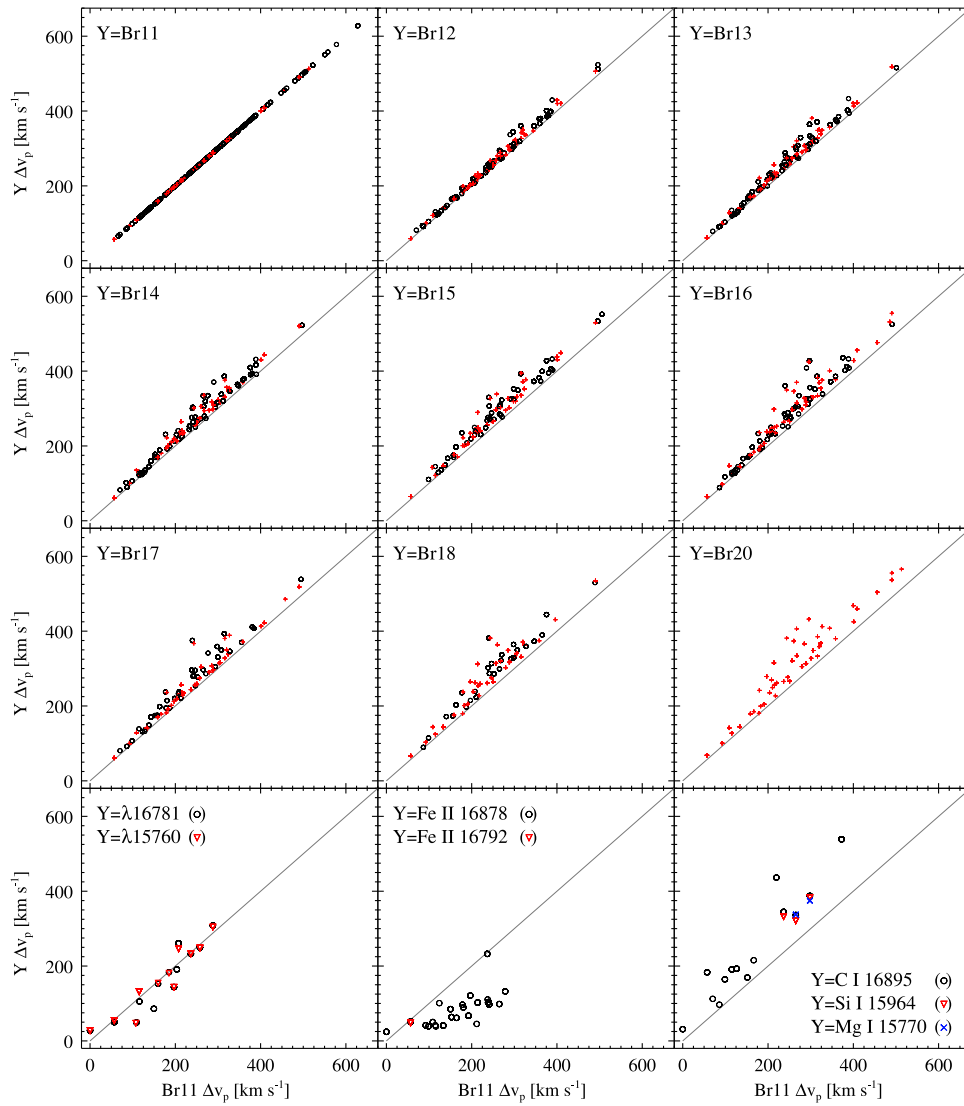


**Figure 12.** Peak separation of Br11 is compared to the peak separations for the other Brackett series lines as well as the most routinely detected metallic emission lines. Symbol meanings are described in Section 5.2.

each star (the number of spectra used for each star is indicated in the “# Obs” column) have been used. The relation in Equation (1) may not necessarily hold for cases of emission lines with asymmetric peak intensities or for shell profiles so these instances have been noted in Table 3. In particular, large  $r_d$  estimates ( $r_d > 5r_*$ ) correspond to asymmetric and shell profiles.

Taking the average of the Br11  $r_d$  estimates for the 19 non-shell stars with roughly symmetric emission peaks, we find an average Br11 formation outer radius and associated standard deviation of

$$r_d(\text{Br11}) = 2.21 \pm 0.73 R_* \quad (2)$$

Hanuschik et al. (1988) found an average  $H\alpha$ -emitting radius of  $\sim 20 R_*$ , while Slettebak et al. (1992) found an average of  $\sim 19 R_*$ . It is important to note, however, that results from interferometry confirm that application of Huang’s law to the double peaks of winebottle-type profiles (appearing for optically thick lines like  $H\alpha$ ) leads to artificially large disk radii estimates (Hummel & Dachs 1992). Interferometric studies typically produce radii estimates of less than  $10 R_*$

over the optical and  $JHK$  bands (see disk radius measurements and papers referenced in Table 2 of (see disk radius measurements and papers referenced in Table 2 of Rivinius et al. 2013b), more similar to what is found here from the Brackett lines.

For  $H\gamma$  and  $\text{Fe II } 6516 \text{ \AA}$ , Slettebak et al. (1992) found emitting radii of  $\sim 7.4 R_*$  and  $\sim 3.9 R_*$  respectively. In a study of optical  $\text{Fe II}$  emission lines for Be stars, Arias et al. (2006) found that, on average, the optical  $\text{Fe II}$  lines are formed at an outer disk radius of 2.0 stellar radii. Therefore, the Br11-emitting outer radius is roughly coincident with the optical  $\text{Fe II}$ -emitting outer radius and well inside the  $H\alpha$ -emitting radius.

Given the sparsity and potential wide-range of quality of  $v \sin i$  information for our sample, disk radii are only estimated for the Br11 and metallic lines. However, it follows from Figure 12 that the Br12–Br20 formation outer radii are interior to that of Br11. Andrillat et al. (1990) and Slettebak et al. (1992) found a correlation between formation location of individual optical lines and the upper energy levels ( $E_k$ ) of the lines. Weaker lines with higher  $E_k$  were generally found to have larger  $\Delta v_p$  and hence smaller  $r_d$ . This is also the case for the

**Table 3**  
Line-emitting Disk Radius Estimates

ABE ID	Lit. $v \sin i$ (km s <sup>-1</sup> )	Ref.	Atom or Ion	# spectra	Mean $\Delta v_p$ (km s <sup>-1</sup> )	Mean $r_d$ ( $R_*$ )
001 <sup>a</sup>	266	9	Br11	4	208	6.56
			$\lambda 15760$	4	246	4.67
			$\lambda 16781$	4	261	4.16
003	225	5	Br11	10	305	2.18
006	231	7	Br11	3	294	2.47
014	230	3	Br11	7	326	1.99
016 <sup>a</sup>	250	4	Br11	1	238	4.43
			Fe II 16878	1	111	20.41
026 <sup>b</sup>	230	3	Br11	12	324	2.02
028	242	4	Br11	12	297	2.66
036 <sup>b</sup>	307	4	Br11	3	456	1.81
046 <sup>b</sup>	235	2	Br11	1	294	2.56
049	120	2	Br11	23	197	1.48
			Fe II 16878	7	67	12.73
067	120	5	Br11	8	133	3.24
			Fe II 16878	8	41	34.32
085	182	8	Br11	4	321	1.29
098	166	11	Br11	1	301	1.21
133 <sup>b</sup>	286	4	Br11	3	285	4.02
138	243	7	Br11	2	365	1.77
140	328	4	Br11	4	382	2.95
165	274	4	Br11	3	397	1.91
167	160	7	Br11	3	300	1.14
170	130	5	Br11	6	153	2.90
			Fe II 16878	6	64	16.76
			C I 16895	2	169	2.36
189	256	6	Br11	5	305	2.81
191	242	4	Br11	1	274	3.11
195 <sup>b</sup>	148	7	Br11	3	266	1.24
A08	343	11	Br11	3	409	2.82
A11	220	7	Br11	3	215	4.19
A12	215	7	Br11	1	358	1.44
A13 <sup>a b</sup>	306	4	Br11	6	257	5.68
			$\lambda 15760$	4	248	6.07
			$\lambda 16781$	4	250	6.00
A15 <sup>a</sup>	350	7	Br11	3	237	8.76
			Fe II 16878	3	232	9.07
			C I 16895	3	345	4.12
			$\lambda 15760$	3	233	9.05
			$\lambda 16781$	3	233	9.04
A17 <sup>b</sup>	300	1	Br11	3	241	6.19
			Fe II 16878	3	102	34.32
A20	210	4	Br11	3	358	1.37
A29 <sup>a</sup>	222	4	Br11	3	197	5.09
			Fe II 16878	3	121	13.42
			$\lambda 15760$	3	144	9.55
			$\lambda 16781$	3	144	9.52
A32	260	10	Br11	3	380	1.87

**References.** (1) Uesugi & Fukuda (1970); (2) Uesugi & Fukuda (1982); (3) Halbedel (1996); (4) Yudin (2001); (5) Abt et al. (2002); (6) Frémat et al. (2005); (7) Frémat et al. (2006); (8) Huang & Gies (2006); (9) Bhavya et al. (2007); (10) Reig et al. (2010); (11) Huang et al. (2010).

<sup>a</sup> Asymmetric emission peak intensities.

<sup>b</sup> Shell stars.

Brackett series lines, where  $E_k$  increases slightly from Br11 to Br20.

A trend toward large  $r_d$  is evident for the Fe II 16878 line with respect to Br11. The average of the five available  $r_d$  estimates for Fe II is  $\sim 19 R_*$ , almost ten times the disk radius

where Br11 is preferentially formed. A consequence of the widely varying formation radii between Br11 and Fe II 16878 is discussed in the following section.

## 6. SINGLE-EPOCH VARIATION IN V/R AND RADIAL VELOCITY

As outlined in Okazaki (1991), long-term V/R variability for Be stars often entails shifts in RV of entire emission line profiles toward whichever peak is stronger at the time and differences in V/R orientation between lines with different formation loci, such that V/R is necessarily constant from atomic species to atomic species or from line to line. These effects are believed to be caused by perturbations with the disks that give rise to one-armed global density waves that slowly precess through the disk with periods averaging 7 years (Rivinius et al. 2013b).

Recent papers discussing the well known Be-shell star  $\zeta$  Tau provided an example of V/R phase lags between Balmer and Brackett series lines and also between individual Brackett series lines. Wisniewski et al. (2007) hypothesized that the optical/NIR phase lag in V/R could be understood in terms of differing preferential formation radii and of the global density perturbation within the disk taking the form of a spiral arm. Štefl et al. (2009) and Carciofi et al. (2009) subsequently showed this to be the case.

### 6.1. H<sub>1</sub> versus H<sub>1</sub> V/R Phase Lags

Evidence of V/R phase lags within the Brackett series lines is present in the spectra for the ABE stars represented in Figure 13. Each Brackett line is displayed individually on a velocity scale in Figure 13 and, with the exception of ABE-A36 (discussed below), the V/R of Br11 for each spectrum is printed in left-most Br11 panels while the differences between the V/R of Br11 and the V/R of Br12–Br20 are printed in the Br12–Br20 panels. For ABE-A29, the V/R orientations progress from V < R at Br11 to V  $\simeq$  R at Br17. The Br19 profile is contaminated by DIB 15271 absorption, but the Br18 and Br20 profiles have V  $\simeq$  R similar to Br17. For ABE-A31 and ABE-181 the opposite progression takes place as the R peak increases in dominance from Br11 to Br20. Although the Br11 profiles for ABE-A36, ABE-A31, and ABE-181 are contaminated by underlying metallic emission ( $\lambda 16781$  and/or Fe II 16878), the V/R phase lag is nonetheless plainly visible from comparison of the Br12 or Br13 profiles to Br20.

Of the 238 stars comprising the ABE sample, ABE-A36 is the only available example of quasi-triple-peaked (*qtp*) Brackett series lines (see upper row of Figure 13), where the “quasi” implies ambiguity as to whether there is actually a true third emission peak or whether instead the central absorption is split into multiple components. The V emission peak of Br11 for ABE-A36 is slightly higher than the R peak due to possible blending with  $\lambda 16781$ , and the possible third peak appears between the dominant outer emission peaks with lesser intensity than those peaks. Br12 is similar in profile to Br11, but from Br12–Br17 the profiles gradually assume a “flat-topped” morphology with the apparent blue central absorption still weakly visible in contrast to the apparent red central absorption having all but disappeared. At Br18, evidence of the third (middle) emission peak emerges again, this time as the dominant peak since the outer V and R peaks have all but disappeared. Br19 is directly

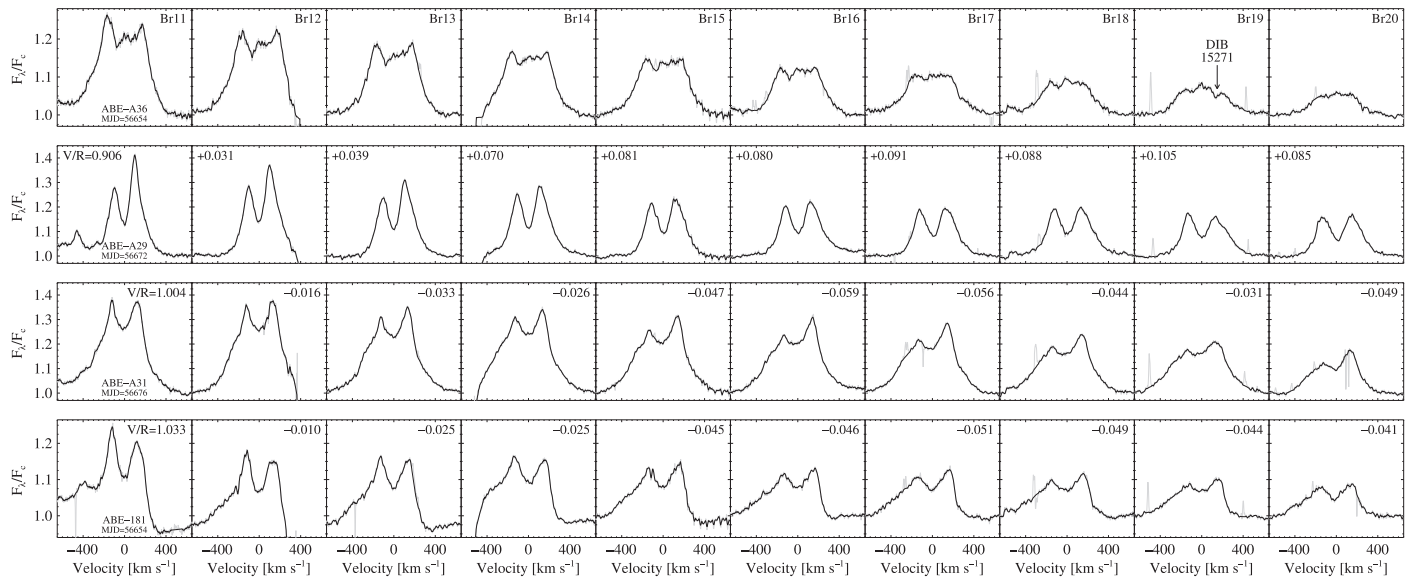


**Figure 13.** Four examples of variation in V/R phase across the Brackett series lines. The Br11 profile for ABE-A36 has a quasi-triple-peaked morphology which gradually becomes a single-peaked morphology at Br20. For ABE-A29, ABE-A31, and ABE-181, the V/R ratio of Br11 is provided in the leftmost panels and subsequent panels provide the difference between the Br12–Br20 V/R ratios and the Br11 V/R ratio. Gradual changes in V/R orientation are seen among Brackett series lines for these stars: blue text for the differences means increasing V/R ratio from Br11 to Br20 (ABE-A29) while red text means decreasing V/R ratio from Br11 to Br20. DIB 15271 absorption is evident on the Br19 line for all four stars.

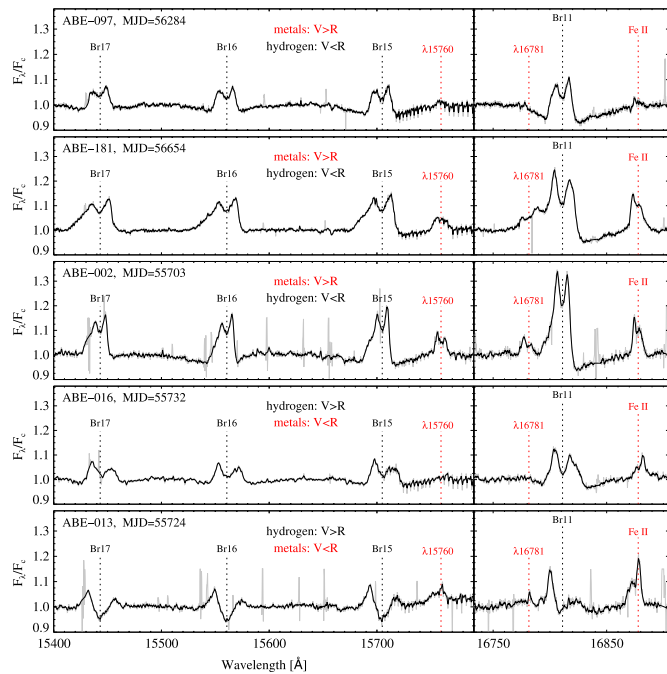


**Figure 14.** H I vs. metallic V/R orientation mismatches are evident in the APOGEE spectra of ABE-097, ABE-181, ABE-002, ABE-016, and ABE-013. The emission wings for ABE-181 and ABE-002 are also clearly extended in the direction of the weaker emission peak for each line, and the metallic emission profiles for ABE-013 appear to be offset in radial velocity from the Brackett lines.

impacted by DIB 15271 but otherwise appears similar to Br18. Finally, the Br20 profile is smooth and rounded with only subtle traces of the blue central absorption and middle “emission peak” (the outer emission peaks are no longer visible).

Steff et al. (2009) pointed out that although *qtp* H $\alpha$  profiles occur at certain times during the V/R cycle of  $\zeta$  Tau, optically

thin lines like O I 8446 and the Brackett series never exhibited any evidence of *qtp*. It is therefore unusual that *qtp* profiles are observed in the Brackett lines for ABE-A36. We can report no additional examples.

## 6.2. H I versus Metallic V/R and RV Phase Lags

The five examples shown in Figure 14 represent the first known examples of disagreement between the V/R orientations of Brackett series versus metallic lines (Fe II 16878,  $\lambda$ 15760, and  $\lambda$ 16781). ABE-097, ABE-181, and ABE-002 have  $V < R$  for H I and  $V > R$  for metallic lines, while ABE-016 and ABE-013 have  $V > R$  for H I and  $V < R$  for metallic lines. Due to the contaminated Br11 profiles for ABE-013, ABE-002, and ABE-181, where the V peak height has been increased by underlying Fe II 16792 emission, the left-hand panels of Figure 14 are extended to encompass not only  $\lambda$ 15760, but also Br15–Br17 to show the typical H I V/R orientation for each star.

Although the lack of available stellar absorption lines means that precise stellar RV determination is not possible, the spectrum for ABE-013 in Figure 14 has been corrected to rest frame based on the average positions of the deep absorptions in the Br12–Br20 lines, while the other spectra lack the deep H I absorptions and therefore were corrected for Doppler shift based on average emission peak shift for the Brackett lines. The result that emerges for ABE-013 is that the Brackett series absorptions do not coincide in RV not with the central depressions in the metallic emission lines as is normally true (see Figure 8), but instead the Brackett series absorptions coincide in RV with the R emission peaks of the metallic lines. More specifically, the Fe II 16878,  $\lambda$ 15760, and  $\lambda$ 16781 profiles are shifted in RV with respect to H I absorption by  $\sim 50$  km s $^{-1}$  in the direction of stronger H I peaks as expected from Okazaki (1991).

ABE-002 and ABE-181 exhibit clear evidence of V/R-related RV shifts in the emission profiles, though of a slightly different variety from that of ABE-013. Metallic and H I

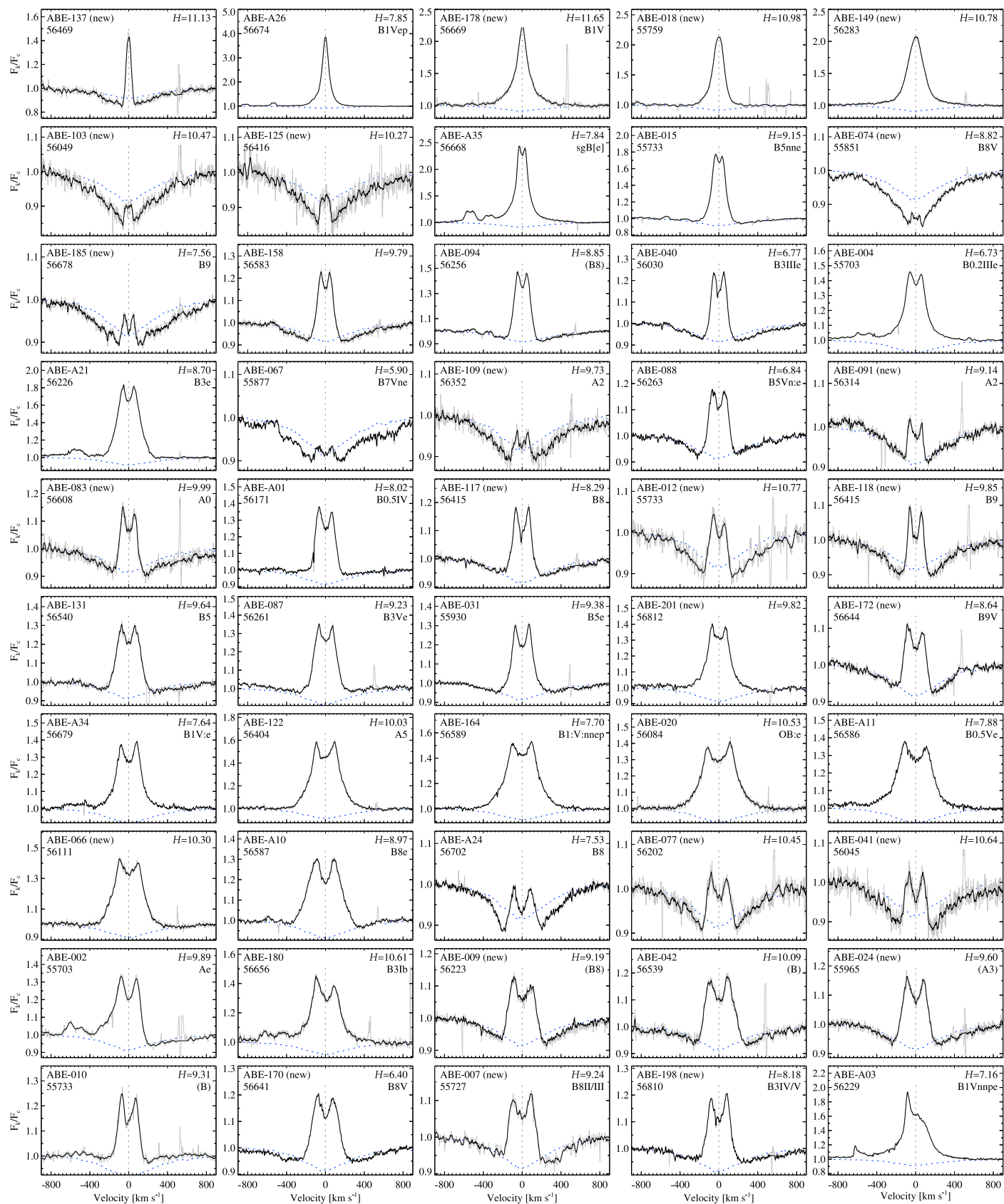


**Figure 15.** Br11 line profiles sorted approximately according to inclination angle, from pole-on to edge-on. ABE identifiers, observation MJDs, 2MASS  $H$  magnitudes, and literature spectral types (where available) are printed in each panel. The average Br11 profile of the quiescent Be stars (ABE-Q01-ABE-Q23) is displayed as a dotted line (blue), and vertical dotted lines (gray) indicate emission peak midpoints or estimated line centers if emission peaks are not present.

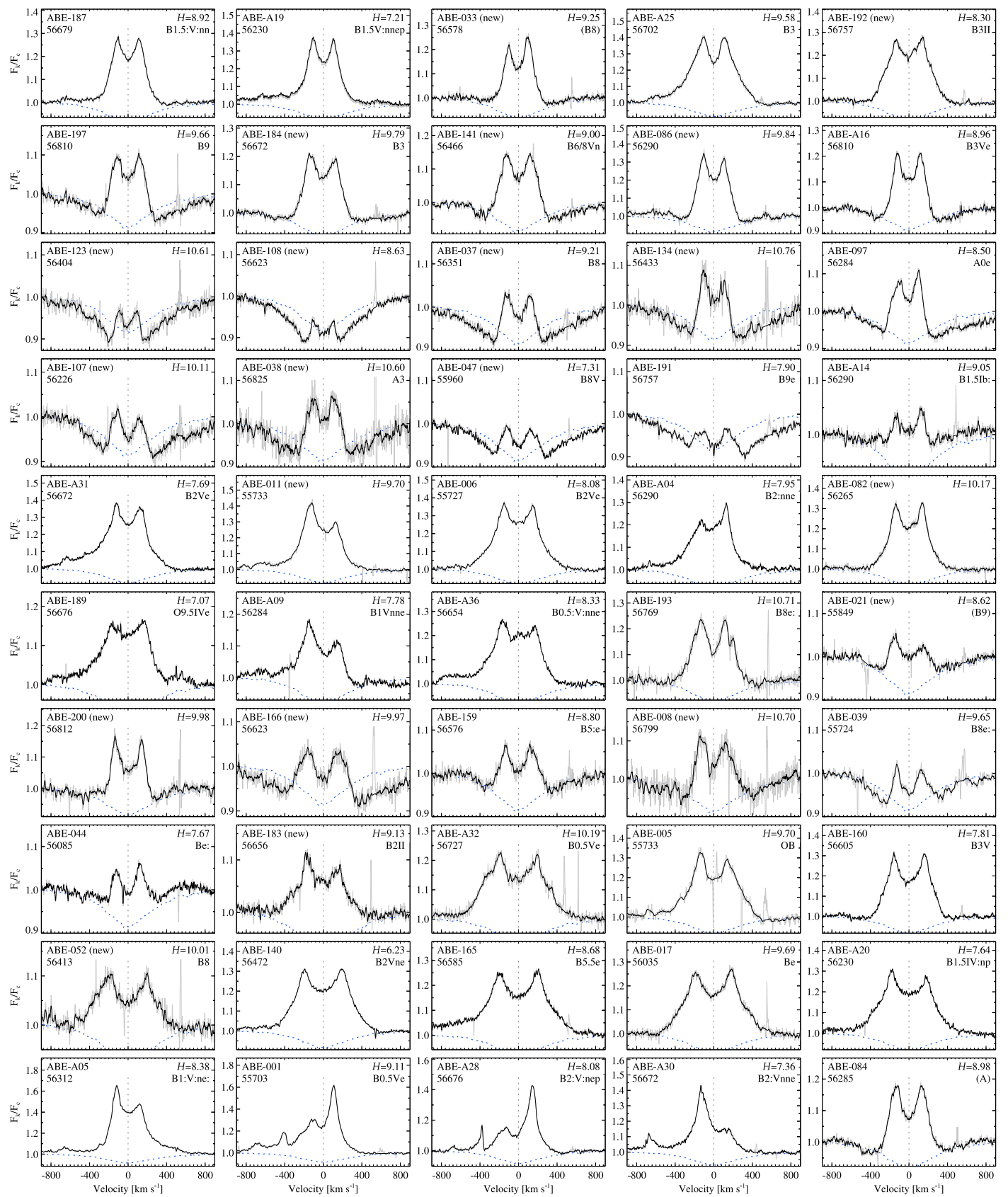


Figure 15. (Continued.)

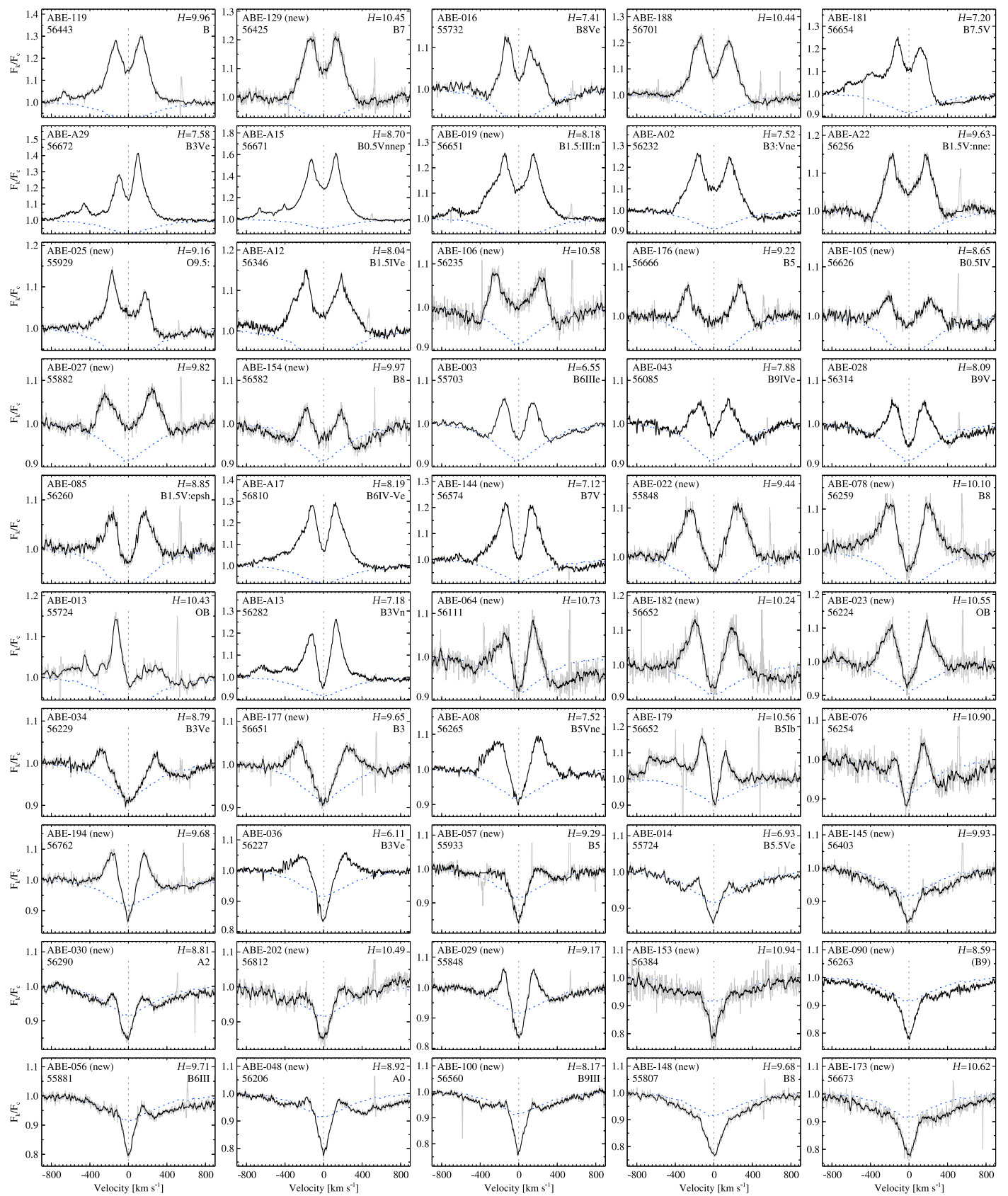


Figure 15. (Continued.)

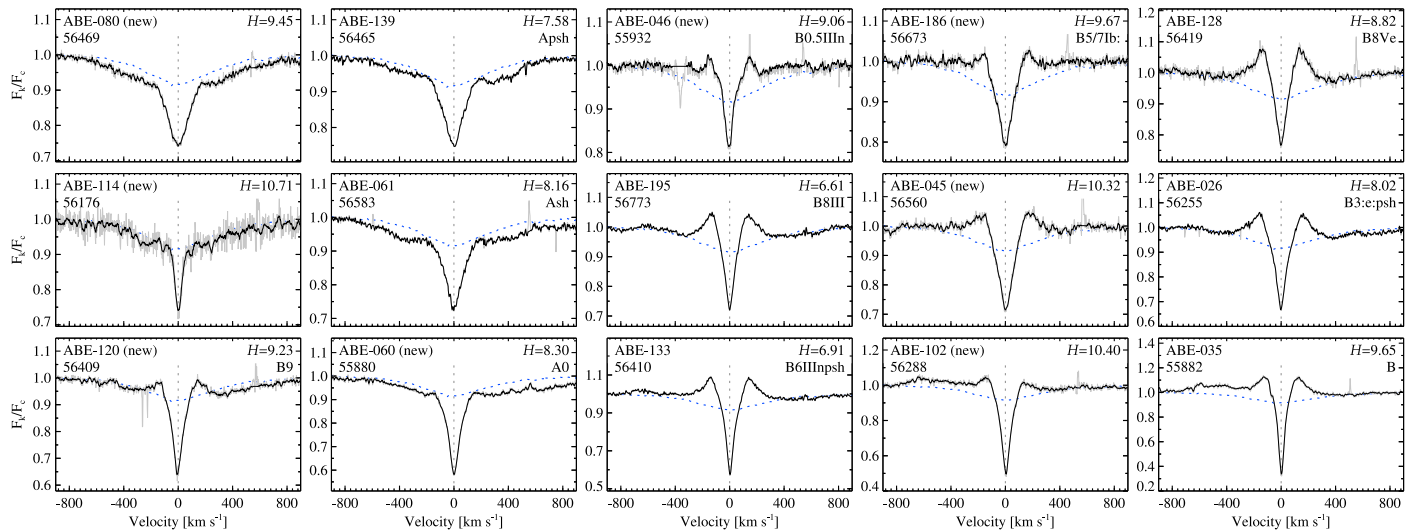


Figure 15. (Continued.)

emission wings for both stars are conspicuously enhanced on the side of the line profiles opposite the stronger emission peak for ABE-002 and ABE-181, with the  $H\text{I}$  wings being enhanced on the blue side and the metallic wings enhanced on the red side. The enhanced blue wings suggest that significantly more emission is being formed in the inner regions of the approaching side of the disk, and the steep declines in intensity, from stronger emission peak to narrower emission base (R side of  $H\text{I}$  for ABE-002 and ABE-181), imply cavities in the inner regions of the receding sides of the disks and relatively increased emission coming from the outer regions of the disks. We interpret these line profiles to suggest more tightly wound spiral patterns to the density oscillation in the disks of these stars versus  $\zeta$  Tau.

## 7. BR11 LINE PROFILES

Br11 line profiles from the highest-quality-available spectrum of each ABE star are displayed in Figure 15. In Figure 15, the Br11 profiles of 165 ABE stars are qualitatively sorted by profile type, going from single-peaked and narrow double-peaked profiles to deep shell profiles. According to the models of Hummel & Dachs (1992) and Hummel & Vrancken (2000), the major line profile shape differences for Be stars are an effect of the inclination angles ( $i$ ) at which the circumstellar disks are observed. Hanuschik et al. (1996) used high-resolution  $H\alpha$  and optical Fe II profiles to devise a Be sub-classification scheme based on the notion of  $i$  dictating to a large extent line profile morphology. Silaj et al. (2010) later showed that line shape in an optically-thick line like  $H\alpha$  is not dictated solely by  $i$  and that very different profile shapes may be observed at fixed  $i$ , but no such investigations of the Brackett series lines have been done.

In sorting the Br11 profiles of the ABE stars according to expected  $i$ , we relied largely on the models of optically thin lines from Hummel & Dachs (1992). The most readily classified Br11 profiles correspond to  $i \sim 0^\circ$  (pole-on), where single-peaked or narrow double-peaked emission is expected, and  $i \sim 90^\circ$  (edge-on), where deep shell absorption with a sharp core (with or without adjacent emission) is expected. The situation is far more ambiguous for profiles corresponding to intermediate  $i$ , but a general trend of increasing central depression depth and overall line width with increasing  $i$  is apparent. Line profiles that could not be satisfactorily sorted by  $i$ , due to weakness or ambiguity of

the disk features, are shown in Figures 16 and 17. Figure 16 profiles are sorted by Br11 peak separation, and Figure 17 profiles are sorted by ABE identifier.

## 8. CONCLUSIONS

SDSS-III/APOGEE has serendipitously provided the first high-resolution view of the  $H$ -band properties of a large number of Be stars, the majority of which are targeted quasi-randomly by the survey as telluric calibrators. Although significant progress has been made toward understanding Be stars over the past few decades via high-resolution optical, interferometric, and spectropolarimetric studies (Rivinius et al. 2013b), any fully explanatory model of the classical Be phenomenon will need to account for the multi-wavelength properties of these stars. Multi-wavelength studies of statistically-significant samples of Be stars are critical yet have historically been few and far between, though the limited exceptions (Clark & Steele 2000; Steele & Clark 2001) have been highly valuable. Due to simultaneous coverage in the  $H$ -band of numerous  $H\text{I}$  lines that are minimally affected by underlying photospheric absorption in comparison to the Balmer series lines, the  $H$ -band is particularly promising in terms of utility toward V/R variability and general Be disk studies. Despite the  $H$ -band covering only a limited number of metallic emission lines, we have shown that the Fe II and Fe II-like ( $\lambda 15760$  and  $\lambda 16781$ ) lines are highly interesting in the context of V/R variability and phase lags between various atomic species.

In the first of a series of papers exploring the  $H$ -band properties of Be stars, we have identified the non-hydrogen emission line content of the ABE star spectra, analyzed the kinematic properties of the metallic and  $H\text{I}$  features, and discussed the more exceptional Be stars within the sample as well as those deviating from the typical emission line content. Further investigation of the identities of emission lines at  $15760 \text{ \AA}$  and  $16781 \text{ \AA}$  is needed, but may require updated atomic line lists. Since little is known about most of the ABE stars themselves, including spectral type and rotation speed, optical follow-up study of these stars is also needed in order to develop a better understanding of  $H$ -band properties as they relate to known stellar parameters.

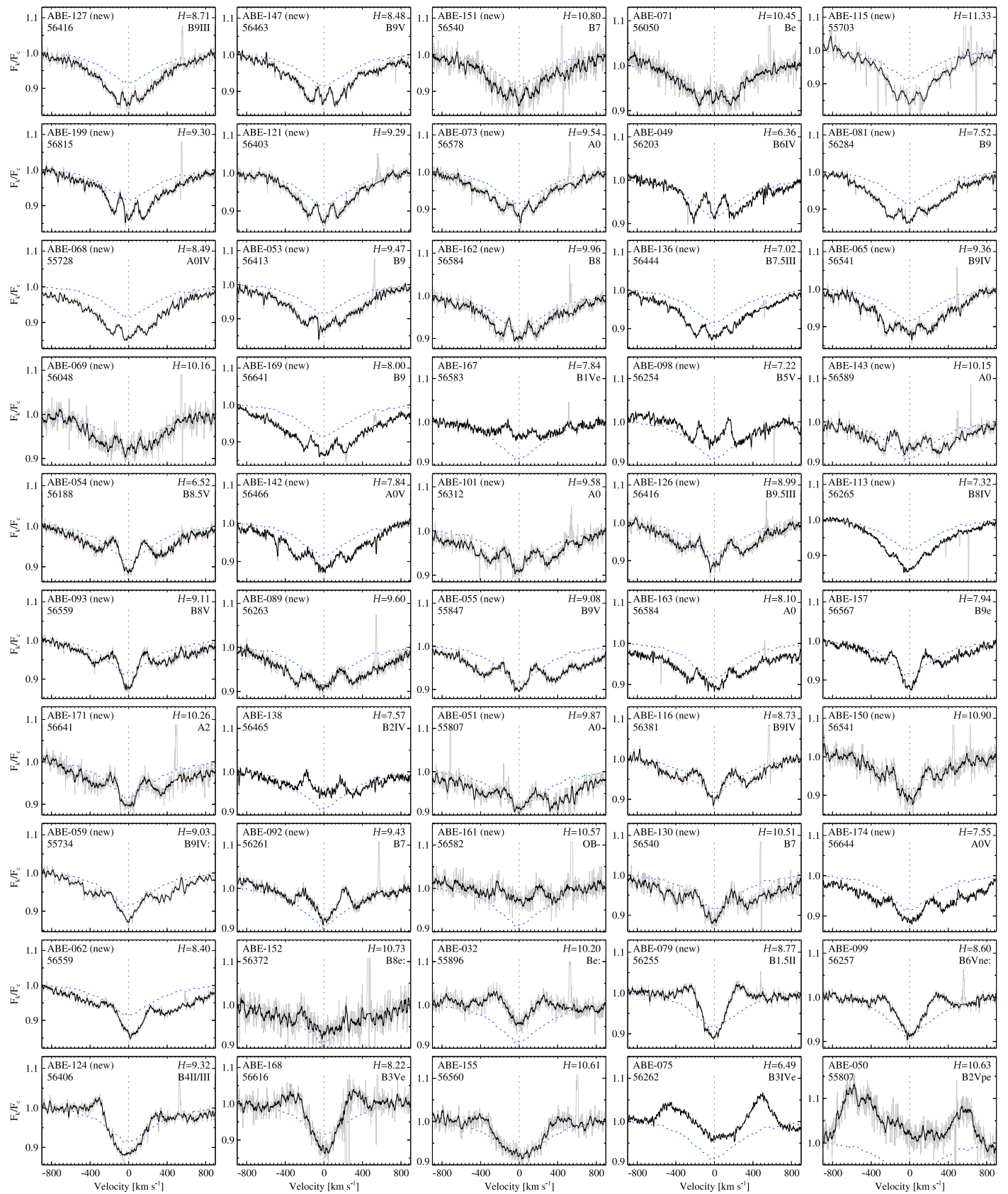


**Figure 16.** Br11 line profiles for stars with weak or ambiguous emission profile type, as well as for the  $\sigma$  Ori E type stars ABE-075 and ABE-050. The panels are sorted by Br11 peak separation. Meanings are otherwise the same as in Figure 15.

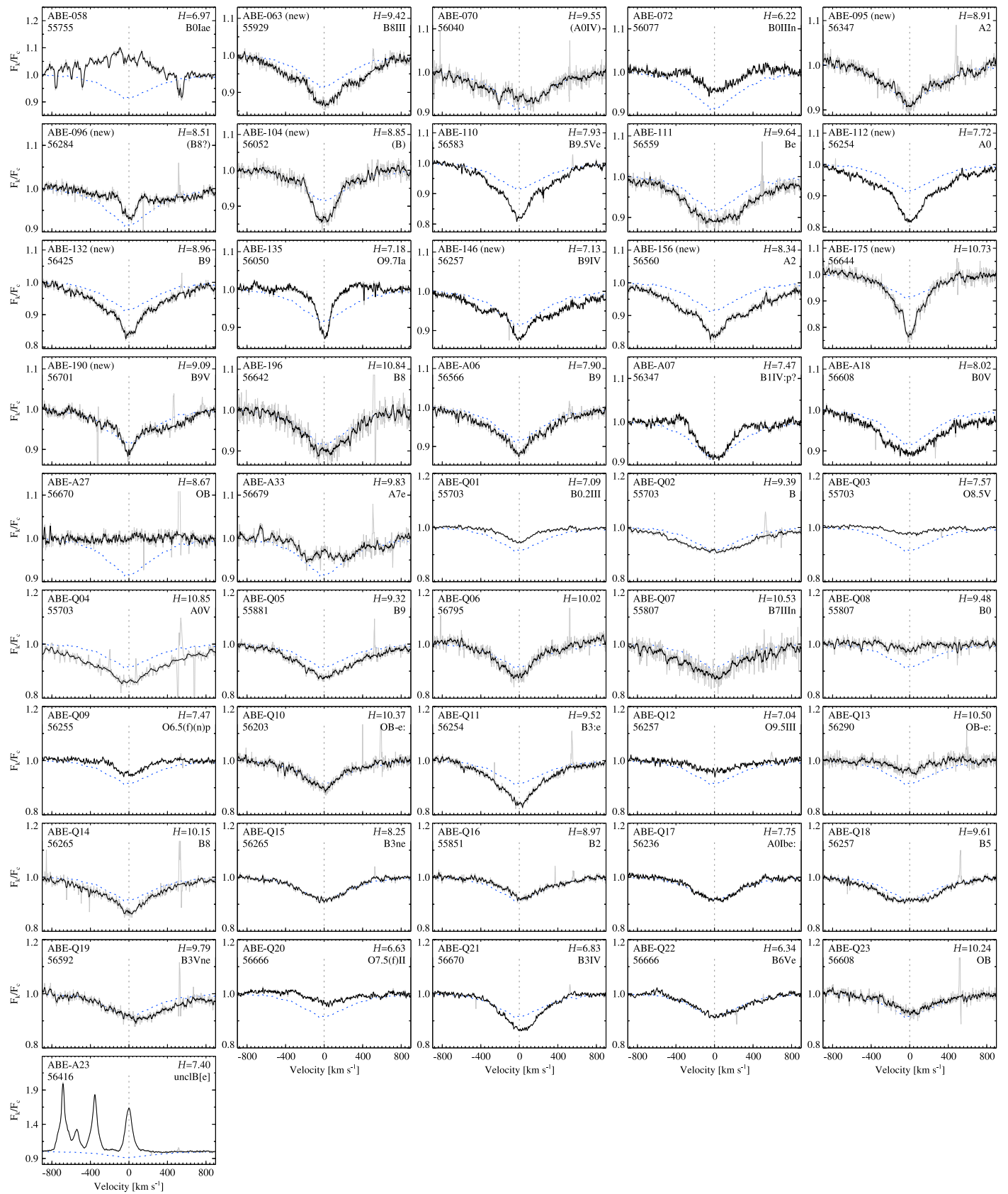


**Figure 17.** Br11 line profiles for stars with weak or ambiguous emission profile type and lack of discernible emission peaks, followed by the sample of previously known emission stars that produced little or no emission in the APOGEE spectra. The panels are mostly sorted by ABE identifier (followed by ABE-A23). Note that the telluric correction is problematic for the plug-plate on which ABE-058 was observed; Br11 is clearly in emission, but the profile is badly contaminated by telluric absorption features. Meanings are otherwise the same as in Figure 15.

**Table A1**  
List of ABE stars

Identifiers				Magnitudes		Spectral type		Line detection or $\Delta v_p$ [km s <sup>-1</sup> ]					
ABE	2MASS	HD	Other	<i>V</i>	<i>H</i>		Ref.	Br11 16811	$\lambda$ 15760	$\lambda$ 16781	Fe II 16792	Fe II 16878	C I 16895
001	20212485 + 3722482	...	VES 203	12.09	9.108	B0.5Ve	74	208	246	261	-	w	-
002	20151525 + 3654562	228576	AS 394	11.41	9.888	Ae	29	152	w	86	-	85	-
003	20162816 + 3703229	192987	HR 7757	6.46	6.548	B6IIIe	22	305	-	-	-	w?	w
004	20234596 + 3830033	229221	MWC 344	9.22	6.734	B0.2IIIe	66	115	131	105	-	w?	191
005	20184170 + 3759106	...	Hen 3-1876	11.37	9.699	OB	6	271	w	w	-	-	-

**References.** (1) Merrill et al. (1942); (2) Cannon & Mayall (1949); (3) Merrill & Burwell (1949); (4) Popper (1950); (5) Miller & Merrill (1951); (6) Nassau & Harris (1952); (7) Morgan et al. (1953); (8) Morgan et al. (1955); (9) Heckmann et al. (1956); (10) Hiltner (1956); (11) Duflot et al. (1958); (12) Alknis (1958); (13) McCuskey (1959); (14) Hardorp et al. (1959); (15) Bouigue et al. (1961); (16) Fehrenbach et al. (1962); (17) Roslund (1963); (18) Feast & Thackeray (1963); (19) McCuskey (1967); (20) Schmidt-Kaler (1967); (21) Racine (1968); (22) Lesh (1968); (23) Guetter (1968); (24) Wackerling (1970); (25) Walborn (1971); (26) Cowley (1972); (27) Lesh & Aizenman (1973); (28) Turner (1976); (29) Henize (1976); (30) Voroshilov et al. (1976); (31) Davis (1977); (32) Christy (1977); (33) Stephenson & Sanduleak (1977); (34) Hill & Lynas-Gray (1977); (35) Stephenson & Sanduleak (1977); (36) Roman (1978); (37) Bartaya (1979); (38) Clausen & Jensen (1979); (39) Ochsenein (1980); (40) Jaschek & Jaschek (1993); (41) Houk (1982); (42) Voroshilov et al. (1985); (43) Bopp (1988); (44) Bidelman (1988); (45) Houk & Smith-Moore (1988); (46) Radoslavova (1989); (47) Sato & Kuji (1990); (48) Turner et al. (1992); (49) Grillo et al. (1992); (50) Turner (1993); (51) Garrison & Gray (1994); (52) Nesterov et al. (1995); (53) Abt & Morrell (1995); (54) Kohoutek & Wehmeyer (1997); (55) Lamers et al. (1998); (56) Esteban & Fernandez (1998); (57) Grenier et al. (1999); (58) Houk & Swift (1999); (59) Yudin (2001); (60) Chauville et al. (2001); (61) Kharchenko (2001); (62) Fabricius et al. (2002); (63) Abt et al. (2002); (64) Miroshnichenko et al. (2003); (65) Hernández et al. (2004); (66) Negueruela (2004); (67) Negueruela et al. (2004); (68) Frémat et al. (2006); (69) Levenhagen & Leister (2006); (70) Uzpén et al. (2007); (71) Reig et al. (2010); (72) Walborn et al. (2010); (73) Sota et al. (2011); (74) Mathew & Subramaniam (2011); (75) Sebastian et al. (2012); (76) Chargeishvili et al. (2013); (77) Eikenberry et al. (2014).

(This table is available in its entirety in machine-readable and Virtual Observatory (VO) forms.)

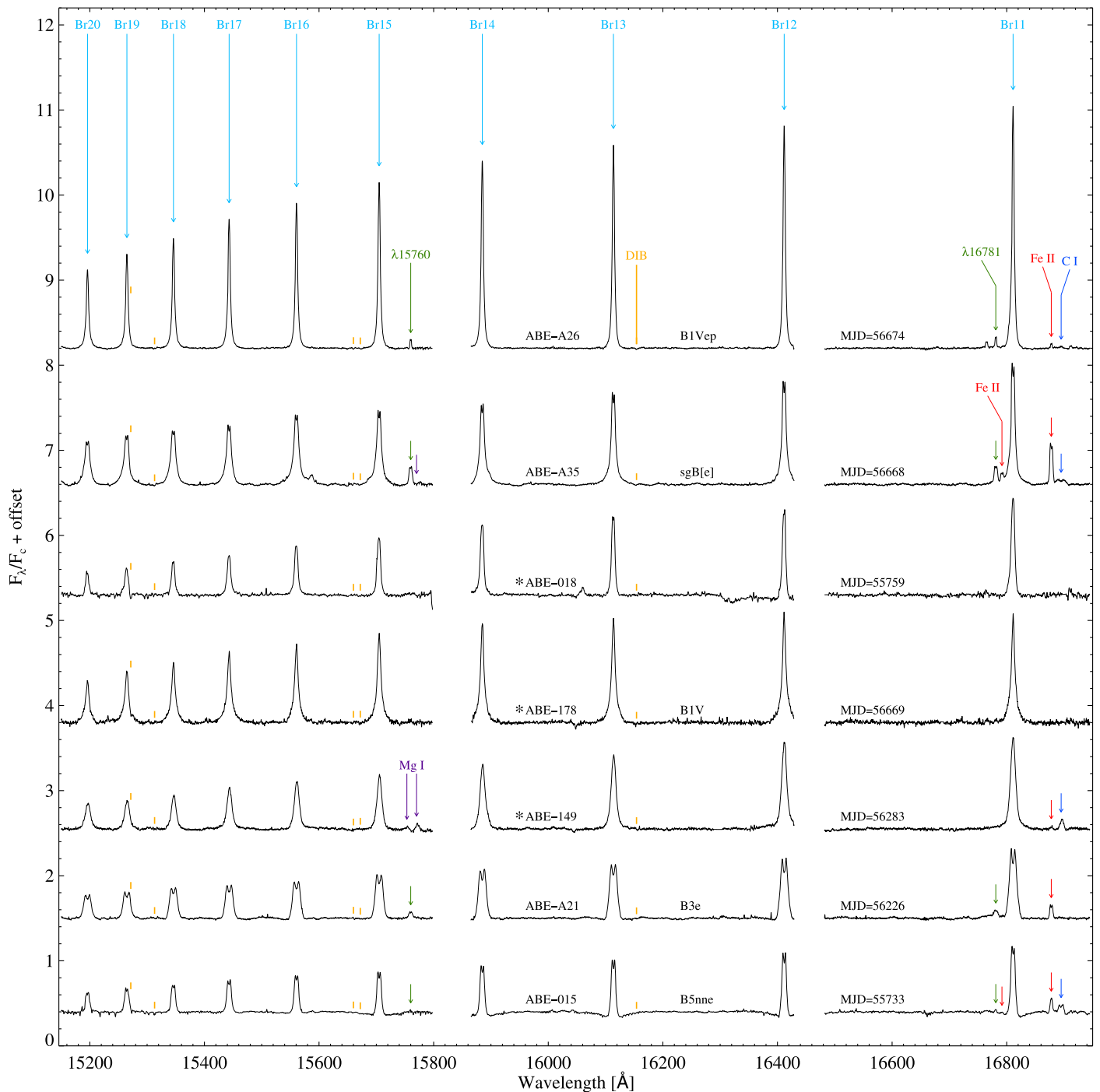


**Figure A1.** APOGEE spectra for Be stars with strong Brackett series emission. The emission lines for ABE-A35, ABE-A21, and ABE-015 are double-peaked, whereas the other stars have single-peaked emission.

## APPENDIX

Full APOGEE spectra for stars with strong Brackett series features are displayed in Figures A1–A3. Shown above each spectrum are ABE identifiers, observation MJDs, and literature spectral types for each star. Newly identified Be stars are indicated with an asterisk before the ABE identifiers. Small line segments mark the positions of the most prominent DIBs

present for some of the stars and arrows mark the positions of the most frequently detected emission lines.

Funding for SDSS-III has been provided by the Alfred P. Sloan Foundation, the Participating Institutions, the National Science Foundation, and the U.S. Department of Energy Office of Science. The SDSS-III web site is <http://www.sdss3.org/>. SDSS-III is managed by the Astrophysical Research Consortium for the Participating Institutions of the SDSS-III Collaboration including

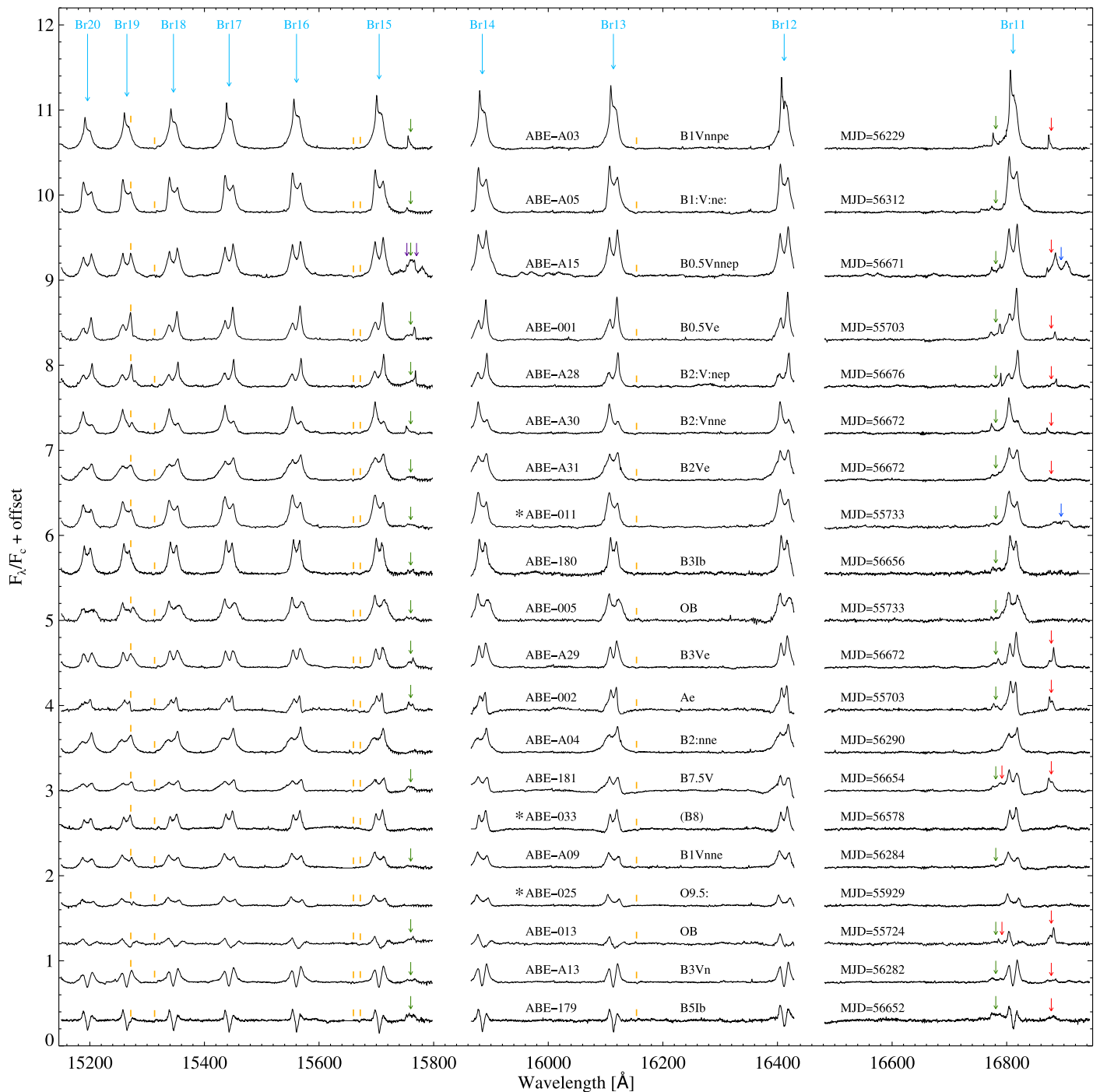


**Figure A2.** APOGEE spectra for a selection of 20 Be stars with asymmetric Brackett series emission. Note the striking similarity between the spectra of ABE-001, ABE-A28, and ABE-A30 (the latter is a V/R reflection of the former two).

the University of Arizona, the Brazilian Participation Group, Brookhaven National Laboratory, Carnegie Mellon University, University of Florida, the French Participation Group, the German Participation Group, Harvard University, the Instituto de Astrofísica de Canarias, the Michigan State/Notre Dame/JINA Participation Group, Johns Hopkins University, Lawrence Berkeley National Laboratory, Max Planck Institute for Astrophysics, Max Planck Institute for Extraterrestrial Physics, New Mexico State University, New York University, Ohio State

University, Pennsylvania State University, University of Portsmouth, Princeton University, the Spanish Participation Group, University of Tokyo, University of Utah, Vanderbilt University, University of Virginia, University of Washington, and Yale University. J. P. W. acknowledges support from NSF-AST 1412110. We thank the anonymous referee and Kevin Covey, both of whom provided feedback that substantially improved the paper. The first author additionally thanks his mother for proofreading drafts of the paper.

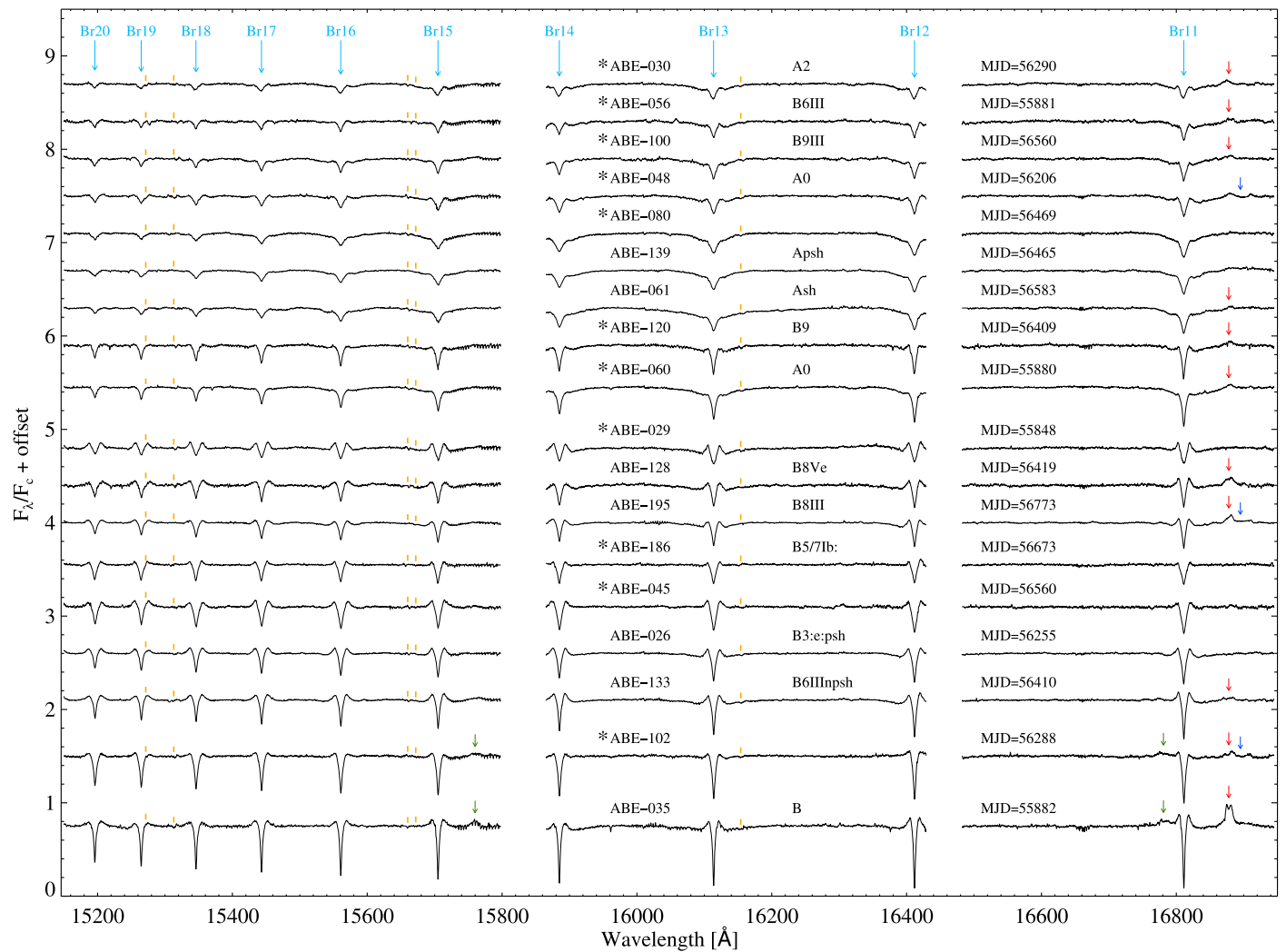


**Figure A3.** APOGEE spectra for a selection of 18 Be-shell stars. Broad photospheric absorption wings are clearly visible in the Brackett lines for the upper nine stars, while the lower nine stars exhibit mostly smooth continua and shell features with adjacent emission.

## REFERENCES

- Abt, H. A., Levato, H., & Grosso, M. 2002, *ApJ*, **573**, 359  
 Abt, H. A., & Morrell, N. I. 1995, *ApJS*, **99**, 135  
 Alknis, A. 1958, *TrRig*, **7**, 33  
 Allen, D. A., & Swings, J. P. 1976, *A&A*, **47**, 293  
 Andriulat, A., Jaschek, M., & Jaschek, C. 1990, *A&AS*, **84**, 11  
 Arias, M. L., Zorec, J., Cidale, L., et al. 2006, *A&A*, **460**, 821  
 Ashok, N. M., & Banerjee, D. P. K. 2000, in *ASP Conf. Ser. 214, The Be Phenomenon in Early-Type Stars*, ed. M. A. Smith et al. (San Francisco, CA: ASP), 468  
 Bartaya, R. A. 1979, *AbaOB*, **51**, 1  
 Bjorkman, K. S., & Miroshnichenko, A. S. 2000, *BAAS*, **32**, 1480  
 Bhavya, B., Mathew, B., & Subramaniam, A. 2007, *BAAS*, **35**, 383  
 Bidelman, W. P. 1988, *PASP*, **100**, 1084  
 Blum, R. D., Ramond, T. M., Conti, P. S., Figer, D. F., & Sellgren, K. 1997, *AJ*, **113**, 1855  
 Bopp, B. W. 1988, *AJ*, **95**, 1543  
 Bouigue, R., Boulon, J., & Pedoussaut, A. 1961, *AnTou*, **28**, 33  
 Cannon, A. J., & Mayall, M. W. 1949, *AnHar*, **112**, 1  
 Carciofi, A. C., Okazaki, A. T., le Bouquin, J.-B., et al. 2009, *A&A*, **504**, 915  
 Carciofi, A. C. 2011, *IAUS*, **272**, 325  
 Chargeishvili, K. B., Bartaya, R. A., & Kharadze, E. K. 2013, *VizieR Online Data Catalog*, **3271**, 0  
 Chauville, J., Zorec, J., Ballereau, D., et al. 2001, *A&A*, **378**, 861  
 Christy, J. W. 1977, *ApJ*, **217**, 127  
 Clark, J. S., & Steele, I. A. 2000, *A&A*, **141**, 65  
 Clausen, J. V., & Jensen, K. S. 1979, *RA*, **9**, 479  
 Covey, K. R., Cottaar, M., Foster, J. B., et al. 2014, *AASM*, **223**, 442.10  
 Cowley, A. 1972, *AJ*, **77**, 750  
 Dachs, J., Hummel, W., & Hanuschik, R. W. 1992, *A&AS*, **95**, 437  
 Davis, R. J. 1977, *ApJ*, **213**, 105  
 Duflot, M., Fehrenbach, C., Duflot, A., Rouviere, E., & Schneider, D. 1958, *JO*, **41**, 43  
 Eikenberry, S. S., Chojnowski, S. D., Wisniewski, J., et al. 2014, *ApJL*, **784**, L30  
 Eisenstein, D. J., Weinberg, D. H., Agol, E., et al. 2011, *AJ*, **142**, 72  
 Esteban, C., & Fernandez, M. 1998, *MNRAS*, **298**, 185  
 Fabricius, C., Makarov, V. V., Knude, J., & Wycoff, G. L. 2002, *A&A*, **386**, 709  
 Feast, M. W., & Thackeray, A. D. 1963, *MmRAS*, **68**, 173  
 Fehrenbach, C., Rebeiro, E., Petit, M., Peyrin, Y., & Monvoisin, C. 1962, *JO*, **45**, 349  
 Frémat, Y., Zorec, J., Hubert, A.-M., & Floquet, M. 2005, *A&A*, **440**, 305  
 Frémat, Y., Neiner, C., Hubert, A.-M., et al. 2006, *A&A*, **451**, 1053  
 Garrison, R. F., & Gray, R. O. 1994, *AJ*, **107**, 1556  
 Geballe, T. R., Najjarro, F., Figer, D. F., Schlegelmilch, B. W., & de La Fuente, D. 2011, *Natur*, **479**, 200  
 Granada, A., Arias, M. L., & Cidale, L. S. 2010, *AJ*, **139**, 1983  
 Gray, R. O., & Corbally, C. J. 2009, *Stellar Spectral Classification*, ed. Richard O. Gray, & Christopher J. Corbally (Princeton, NJ: Princeton Univ. Press)

- Greenstein, J. L., & Wallerstein, G. 1958, *ApJ*, **127**, 237
- Grenier, S., Baylac, M.-O., Rolland, L., et al. 1999, *A&AS*, **137**, 451
- Grillo, F., Sciortino, S., Micela, G., Vaiana, G. S., & Harnden, F. R., Jr. 1992, *ApJS*, **81**, 795
- Groh, J. H., Daminieli, A., & Jablonski, F. 2007, *A&A*, **465**, 993
- Guetter, H. H. 1968, *PASP*, **80**, 197
- Gunn, J. E., Siegmund, W. A., Mannery, E. J., et al. 2006, *AJ*, **131**, 2332
- Halbedel, E. M. 1996, *PASP*, **108**, 833
- Hamann, F., Depoy, D. L., Johansson, S., & Elias, J. 1994, *ApJ*, **422**, 626
- Hanuschik, R. W. 1987, *A&A*, **173**, 299
- Hanuschik, R. W. 1988, *A&A*, **190**, 187
- Hanuschik, R. W., Kozok, J. R., & Kaiser, D. 1988, *A&A*, **189**, 147
- Hanuschik, R. W., Hummel, W., Sutorius, E., Dietle, O., & Thimm, G. 1996, *A&AS*, **116**, 309
- Hanuschik, R. W. 1996, *A&A*, **308**, 170
- Hardorp, J., Rohlf, K., Slettebak, A., & Stock, J. 1959, *LS*, **0**,
- Heckmann, O., Dieckvoss, W., & Kox, H. 1956, *AN*, **283**, 109
- Heintz, W. D. 1998, *ApJS*, **117**, 587
- Henize, K. G. 1976, *ApJS*, **30**, 491
- Hernández, J., Calvet, N., Briceño, C., Hartmann, L., & Berlind, P. 2004, *AJ*, **127**, 1682
- Hill, P. W., & Lynas-Gray, A. E. 1977, *MNRAS*, **180**, 691
- Hiltner, W. A. 1947, *ApJ*, **105**, 212
- Hiltner, W. A. 1956, *ApJS*, **2**, 389
- Hony, S., Waters, L. B. F. M., Zaaf, P. A., et al. 2000, *A&A*, **355**, 187
- Horne, K., & Marsh, T. R. 1986, *MNRAS*, **218**, 761
- Houk, N., & Smith-Moore, M. 1988, Michigan Catalogue of Two-dimensional Spectral Types for the HD Stars. (Ann Arbor, MI: Univ. of Michigan)
- Houk, N., & Swift, C. 1999, in Michigan Catalogue of Two-dimensional Spectral Types for the HD Stars. (Ann Arbor, MI: Univ. of Michigan)
- Houk, N. 1982, Michigan Catalogue of Two-dimensional Spectral Types for the HD stars. (Ann Arbor, MI: Univ. of Michigan)
- Huang, S.-S. 1972, *ApJ*, **171**, 549
- Huang, W., Gies, D. R., & McSwain, M. V. 2010, *ApJ*, **722**, 605
- Huang, W., & Gies, D. R. 2006, *ApJ*, **648**, 580
- Hummel, W., & Dachs, J. 1992, *A&A*, **262**, L17
- Hummel, W., & Vrancken, M. 2000, *A&A*, **359**, 1075
- Jaschek, C., & Jaschek, M. 1993, *A&AS*, **97**, 807
- Kendall, T. R., de Wit, W. J., & Yun, J. L. 2003, *A&A*, **408**, 313
- Kharchenko, N. V. 2001, *KFNT*, **17**, 409
- Kohoutek, L., & Wehmeyer, R. 1997, *AAHam* **11**
- Kramida, A., Ralchenko, Yu., & Reader, J. 2013, NIST ASD Team, NIST Atomic Spectra Database, (version 5.1), [Online]. Available: <http://physics.nist.gov/asd> [Thursday, 26-Dec-2013 13:32:45 EST]. National Institute of Standards and Technology, Gaithersburg, MD.
- Kraus, S., Calvet, N., Hartmann, L., et al. 2012, *ApJ*, **752**, 11
- Lamers, H. J. G. L. M., Zickgraf, F.-J., de Winter, D., Houziaux, L., & Zorec, J. 1998, *A&A*, **340**, 117
- Lee, U., Osaki, Y., & Saio, H. 1991, *MNRAS*, **250**, 432
- Lesh, J. R., & Aizenman, M. L. 1973, *A&A*, **22**, 229
- Lesh, J. R. 1968, *ApJS*, **17**, 371
- Levenhagen, R. S., & Leister, N. V. 2006, *MNRAS*, **371**, 252
- Majewski, S. R. 2012, *AASM*, **219**, 205.06
- Mathew, B., & Subramaniam, A. 2011, *BASI*, **39**, 517
- Mathew, B., Banerjee, D. P. K., Naik, S., & Ashok, N. M. 2012, *MNRAS*, **423**, 2486
- McCuskey, S. W. 1959, *ApJS*, **4**, 1
- McCuskey, S. W. 1967, *AJ*, **72**, 1199
- McSwain, M. V., Huang, W., & Gies, D. R. 2009, *ApJ*, **700**, 1216
- Meillard, A., Stee, P., Vannier, M., et al. 2007, *A&A*, **464**, 59
- Mennickent, R. E., Sabogal, B., Granada, A., & Cidale, L. 2009, *PASP*, **121**, 125
- Merrill, P. W., & Burwell, C. G. 1949, *ApJ*, **110**, 387
- Merrill, P. W., Burwell, C. G., & Miller, W. C. 1942, *ApJ*, **96**, 15
- Meyer, M. R., Edwards, S., Hinkle, K. H., & Strom, S. E. 1998, *ApJ*, **508**, 397
- Miller, W. C., & Merrill, P. W. 1951, *ApJ*, **113**, 624
- Miroshnichenko, A. S., Kusakin, A. V., Bjorkman, K. S., et al. 2003, *A&A*, **412**, 219
- Morgan, W. W., Whitford, A. E., & Code, A. D. 1953, *ApJ*, **118**, 318
- Morgan, W. W., Code, A. D., & Whitford, A. E. 1955, *ApJS*, **2**, 41
- Murdoch, K. A., Drew, J. E., & Anderson, L. S. 1994, *A&A*, **284**, 27
- Nassau, J. J., & Harris, D., III 1952, *ApJ*, **115**, 459
- Negueruela, I. 2004, *AN*, **325**, 380
- Negueruela, I., Steele, I. A., & Bernabeu, G. 2004, *AN*, **325**, 749
- Neiner, C., de Batz, B., Cochard, F., et al. 2011, *AJ*, **142**, 149
- Nesterov, V. V., Kuzmin, A. V., Ashimbaeva, N. T., et al. 1995, *A&AS*, **110**, 367
- Ochsenbein, F. 1980, *BICDS*, **19**, 74
- Okazaki, A. T. 1991, *PASJ*, **43**, 75
- Oksala, M. E., Kraus, M., Cidale, L. S., Muratore, M. F., & Borges Fernandes, M. 2013, *A&A*, **558**, A17
- Polidan, R. S., & Peters, G. J. 1976, in IAU Symp. 70, Be and Shell Stars, ed. A. Slettebak (Boston, MA: Reidel), 59
- Popper, D. M. 1950, *ApJ*, **111**, 495
- Porter, J. M., & Rivinius, T. 2003, *PASP*, **115**, 1153
- Racine, R. 1968, *AJ*, **73**, 233
- Radoslavova, T. 1989, *AN*, **310**, 223
- Reig, P., Zezas, A., & Gkouvelis, L. 2010, *A&A*, **522**, A107
- Renson, P., Gerbaldi, M., & Catalano, F. A. 1991, *A&AS*, **89**, 429
- Rivinius, T., Štefl, S., & Baade, D. 2006, *A&A*, **459**, 137
- Rivinius, T. 2013, Stellar Pulsations: Impact of New Instrumentation and New Insights, **31**, 253
- Rivinius, T., Carciofi, A. C., & Martayan, C. 2013, *A&ARv*, **21**, 69
- Rivinius, T., Baade, D., Townsend, R. H. D., Carciofi, A. C., & Štefl, S. 2013, *A&A*, **559**, L4
- Roman, N. G. 1978, *AJ*, **83**, 172
- Roslund, C. 1963, *ArA*, **3**, 97
- Rudy, R. J., Erwin, P., Rossano, G. S., & Puetter, R. C. 1992, *ApJ*, **398**, 278
- Sato, K., & Kuji, S. 1990, *A&AS*, **85**, 1069
- Schmidt-Kaler, T. 1967, *PASP*, **79**, 181
- Sebastian, D., Guenther, E. W., Schaffenroth, V., et al. 2012, *A&A*, **541**, A34
- Silaj, J., Jones, C. E., Tycner, C., Sigut, T. A. A., & Smith, A. D. 2010, *ApJS*, **187**, 228
- Skiff, B. A. 2013, VizieR Online Data Catalog, **1**, 2023
- Skrutskie, M. F., Cutri, R. M., Stiening, R., et al. 2006, *AJ*, **131**, 1163
- Slettebak, A., Collins, G. W. II, & Truax, R. 1992, *ApJS*, **81**, 335
- Smak, J. 1969, *ACA*, **19**, 155
- Smak, J. 1969, *ACA*, **31**, 395
- Smee, S. A., Gunn, J. E., Uomoto, A., et al. 2013, *AJ*, **146**, 32
- Smith, N. 2001, Eta Carinae and Other Mysterious Stars: The Hidden Opportunities of Emission Spectroscopy, **242**, 81
- Smith, N., & Davidson, K. 2001, *ApJL*, **551**, 401
- Sota, A., Maiz Appelániz, J., Walborn, N. R., Alfaro, E. J., Barbá, R. H., Morrell, N. I., Gamero, R. C., & Arias, J. L. 2011, *ApJS*, **193**, 24
- Steele, I. A., Negueruela, I., & Clark, J. S. 1999, *A&AS*, **137**, 147
- Steele, I. A., & Clark, J. S. 2001, *A&A*, **371**, 643
- Štefl, S., Rivinius, T., Carciofi, A. C., et al. 2009, *A&A*, **504**, 929
- Stephenson, C. B., & Sanduleak, N. 1977, *PW&SO*, **2**, 71
- Stephenson, C. B., & Sanduleak, N. 1977, *ApJS*, **33**, 459
- Strom, S. E., Wolff, S. C., & Dror, D. H. A. 2005, *AJ*, **129**, 809
- Struve, O. 1931, *ApJ*, **74**, 225
- Townsend, R. H. D., & Owocki, S. P. 2005, *MNRAS*, **357**, 251
- Townsend, R. H. D., Owocki, S. P., & Groote, D. 2005, *ApJL*, **630**, L81
- Turner, D. G., Forbes, D., & Pedreros, M. 1992, *AJ*, **104**, 1132
- Turner, D. G. 1976, *ApJ*, **210**, 65
- Turner, D. G. 1993, *A&AS*, **97**, 755
- Tuthill, P. G., & Lloyd, J. P. 2007, *Sci*, **316**, 247
- Uesugi, A., & Fukuda, I. 1970, Catalogue of Rotational Velocities of the Stars, (Kyoto: Univ. of Kyoto)
- Uesugi, A., & Fukuda, I. 1982, Catalogue of Stellar Rotational Velocities, (rev. ed.; Kyoto: Univ. of Kyoto)
- Uzpen, B., Kobulnicky, H. A., Monson, A. J., et al. 2007, *ApJ*, **658**, 1264
- Voroshilov, V. I., Guseva, N. G., Kalandadze, N. B., et al. 1976, *KiIND*
- Voroshilov, V. I., Guseva, N. G., Kalandadze, N. B., et al. 1985, *KiIND* **140** In Russian
- Wackerling, L. R. 1970, *MmRAS*, **73**, 153
- Walborn, N. R., Howarth, I. D., Evans, C. J., et al. 2010, *AJ*, **139**, 1283
- Walborn, N. R. 1971, *ApJS*, **23**, 257
- Wheelwright, H. E., Bjorkman, J. E., Oudmaier, R. D., et al. 2012, *MNRAS*, **423**, L11
- Wilson, J. C., Hearty, F., Skrutskie, M. F., et al. 2010, *Proc. SPIE*, **7735**, 77351C
- Wisniewski, J. P., Kowalski, A. F., Bjorkman, K. S., Bjorkman, J. E., & Carciofi, A. C. 2007, *ApJ*, **656**, 21
- Wisniewski, J. P., Draper, Z. H., Bjorkman, K. S., et al. 2010, *ApJ*, **709**, 1306
- Yudin, R. V. 2001, *A&A*, **368**, 912
- Zasowski, G., Johnson, J. A., Frinchaboy, P. M., et al. 2013, *AJ*, **146**, 81
- Zasowski, G., Ménard, B., Bizyaev, D., et al. 2014, arXiv:14061195